Protist, Vol. 170, 259–282, July 2019
http://www.elsevier.de/protis
Published online date 13 April 2019

Protist

ORIGINAL PAPER

Morphological, Ultrastructural, Motility and Evolutionary Characterization of Two New Hemistasiidae Species

Galina Prokopchuk[a,2], Daria Tashyreva[a,2], Akinori Yabuki[b], Aleš Horák[a,c], Petra Masařová[a], and Julius Lukeš[a,c,1]

[a]Biology Centre, Institute of Parasitology, Czech Academy of Sciences, České Budějovice (Budweis), Czech Republic
[b]Department of Marine Diversity, Japan Agency for Marine-Earth Science and Technology, Yokosuka, Japan
[c]Department of Molecular Biology and Genetics, Faculty of Science, University of South Bohemia, České Budějovice (Budweis), Czech Republic

Submitted December 4, 2018; Accepted April 4, 2019
Monitoring Editor: Dmitri Maslov

Until now, *Hemistasia phaeocysticola* was the only representative of the monogeneric family Hemistasiidae available in culture. Here we describe two new axenized hemistasiids isolated from Tokyo Bay, Japan. Like in other diplonemids, cellular organization of these heterotrophic protists is characterized by a distinct apical papilla, a tubular cytopharynx contiguous with a deep flagellar pocket, and a highly branched mitochondrion with lamellar cristae. Both hemistasiids also bear a prominent digestive vacuole, peripheral lacunae, and paraflagellar rods, are highly motile and exhibit diverse morphologies in culture. We argue that significant differences in molecular phylogenetics and ultrastructure between these new species and *H. phaeocysticola* are on the generic level. Therefore, we have established two new genera within Hemistasiidae – *Artemidia* gen. n. and *Namystynia* gen. n. to accommodate *Artemidia motanka*, sp. n. and *Namystynia karyoxenos*, sp. n., respectively. *A. motanka* permanently carries tubular extrusomes, while in *N. karyoxenos*, they are present only in starving cells. An additional remarkable feature of the latter species is the presence, in both the cytoplasm and the nucleus, of the endosymbiotic rickettsiid *Candidatus* Sneabacter namystus.

Key words: Diplonemids; Hemistasiidae; rickettsiid; endosymbiosis; extrusome.

Introduction

Since its initial description more than 100 years ago, the taxonomic position of the genus *Hemistasia* remained under debate. Based on its morphological and ultrastructural features, this enigmatic marine protist has been initially considered to be a dinoflagellate (Pavillard 1922; Scherffel 1900), a euglenoid (Griessmann 1913) or, until recently, a kinetoplastid (Elbrächter et al. 1996; Senn 1911). However, a closer inspection of its ultrastructural features associated *Hemistasia* with another group within the phylum Euglenozoa, namely the diplonemids (Simpson 1997). Indeed, large mitochondrial

[1]Corresponding author;
[2]Equal contribution.
e-mail jula@paru.cas.cz (J. Lukeš).

https://doi.org/10.1016/j.protis.2019.04.001

cristae, a distinctive apical papilla, two parallel flagella that emerge from a deep subapical flagellar pocket, and an adjacent tubular feeding apparatus including vanes with fuzzy coats supported this inference (Elbrächter et al. 1996; Simpson and Roger 2004).

The application of 18S rRNA gene sequence analysis terminated the controversy and solidified the affiliation of *Hemistasia* with the diplonemids (Flegontova et al. 2016; Yabuki and Tame 2015). Ultimately, due to its phylogenetic distance from the core diplonemids, *Hemistasia* was endowed with a new family within the order Diplonemida (Adl et al. 2019; Cavalier-Smith 2016; Yabuki and Tame 2015) and became a sister group to the clade incorporating the recently established Eupelagonemidae, and the deep-sea pelagic diplonemids (DSPD) clade II (Flegontova et al. 2016; Lara et al. 2009; Lukeš et al. 2015; Okamoto et al. 2019).

The family Hemistasiidae is currently monogeneric, with the genus *Hemistasia* containing a single recognized species, *Hemistasia phaeocysticola* (Cavalier-Smith 2016; Elbrächter et al. 1996; Griessmann 1913). Although Lee (2002) moved *Phyllomitus amylophagus* to the genus *Hemistasia*, thus creating the new combination *Hemistasia amylophagus*, Cavalier-Smith (2016) later argued against it, as this protist possesses a nemadesm and lacks swollen peripheral lacunae. Hence, *H. phaeocysticola* remain the only representative of the non-classical diplonemids that is available in culture and has been formally described based on light microscopy, ultrastructure and molecular data (Elbrächter et al. 1996; Yabuki and Tame 2015).

Recent global environmental surveys of marine microeukaryotes, performed by the *Tara* Oceans expedition, documented a high abundance and extreme diversity of diplonemids (David and Archibald 2016; de Vargas et al. 2015; Gawryluk et al. 2016). A dedicated analysis of the diplonemid V9 18S rRNA barcodes extracted from the surveys revealed over 2,000 putative *Hemistasia* ribotypes, most of which seem to have a cosmopolitan distribution (Flegontova et al. 2016). However, at present we can only speculate about the life style, cell biology, ecology and the role of these so far overlooked taxa in the ecosystem. The available data indicate that hemistasiids inhabit predominantly coastal waters and appear to be eukaryovores and/or detritivores, likely feeding on various marine planktonic invertebrates, protists and algae (Elbrächter et al. 1996; Elbrächter and Schnepf 1998; Flegontova et al. 2016).

While exploring the surface waters of Tokyo Bay, Japan, we have collected and subsequently established axenic cultures of two new species, which branch at the base of the family Hemistasiidae in 18S rRNA gene phylogenies. In this study, we provide a comprehensive description of their morphology and behavior under culture conditions. This is another step on the long path to improve our extremely limited knowledge about the structural diversity, evolutionary history, and life strategies of diplonemids, and hemistasiids in particular.

Results

Light and Fluorescence Microscopy

Namystynia karyoxenos (YPF 1621) gen. n., sp. n.

Within a single batch culture, the cell size varies greatly, from 13 to 27 μm in length and 4 to 8 μm in width (mean ± SD of 20.3 ± 4 μm × 5.5 ± 0.9 μm; n = 37). The predominant morphotype is represented by long cylindrical swimming cells with round posterior end and highly asymmetric apex (Fig. 1A–D). The anterior portion is marked by a pronounced subapical depression that forms the anterior part of the spiral groove (Fig. 1A–B; see below); at some angles and planes, the protruding part can be seen as a pointy rostrum (Fig. 1E), at the tip of which is a long and flexible apical papilla, a hallmark of diplonemids (Fig. 1F). Two parallel flagella are inserted sub-apically into the groove (Fig. 1A–C). The groove starts above the flagellar attachment area (Fig. 1C) and runs halfway down the cell in a spiral course (Fig. 1D). The flagella are unequal and heterodynamic, and both are thick and longer than the cell body (Fig. 1G). The swimming cells usually contain small vacuoles scattered throughout the cytoplasm (Fig. 1A–D, G) along with a single medium-sized digestion vacuole in their posterior part (data not shown). Less commonly, they carry a conspicuously large posterior vacuole that gives them a pear-shaped appearance (Fig. 1E). In rare cases, the vacuole can take up more than 2/3 of the cell volume. However, this feature becomes common among cells following cryopreservation in liquid nitrogen (data not shown). Numerous round inclusions, possibly storage products, are sometimes also seen (Fig. 1H). In small cells, flagella occasionally appear to be inserted centrally (Fig. 1F), apparently due to a significant reduction of the posterior half. Spherical sessile stages with both flagella coiled around the anterior region of the cell are frequent in both fresh and old batch cultures (Fig. 1I).

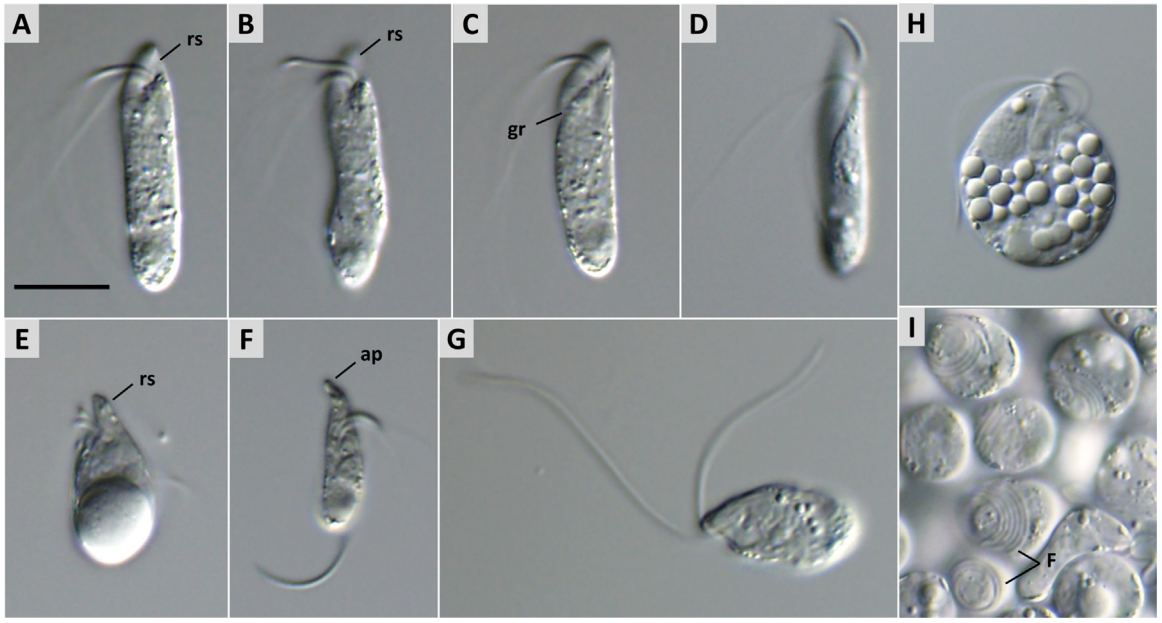

Figure 1. Differential interference contrast micrographs of *Namystynia karyoxenos* YPF 1621, n. gen., n. sp. cultured in artificial seawater medium. (**A–D)** Typical cylindrical swimming cell showing highly asymmetric apex and a spiral groove (gr) that extends halfway down the cell. (**E**) Rounded cell with big posterior vacuole and anterior portion with papilla, seen as rostrum (rs). (**F**) Small cell with protruding apical papilla (ap) and flagella inserted centrally. (**G–H**) Compressed cells showing long subequal flagella and plentiful round inclusions. (**I**) Cluster of spherical sessile cells with both flagella (F) wrapped around cell anterior. Scale bar: 10 μm.

The cells are highly metabolic, which is displayed by contraction-expansion cycles and twisting movements of the entire body (Supplementary Material Video 1). In addition, the protruding anterior part ("rostrum") is able to flex back and forth independently from the rest of the cell (Supplementary Material Video 2). During swimming, cells oscillate around their longitudinal axis, rotate and change their swimming direction either smoothly or abruptly (Supplementary Material Videos 3 and 4).

After being placed under unfavorable conditions, such as increased temperature or salinity (observed by light microscopy in a drying drop), the peripheral lacunae become visible (Supplementary Material Video 5), which increasingly swell with time. Eventually, the cytoplasm shrinks into a small volume surrounded by transparent lacunae that contain rapidly moving rectangular light-refracting particles (Supplementary Material Video 5). The content of the lacunae can be later expelled from the posterior half of the cell (Supplementary Material Video 6). It appears that the lacunae can enlarge passively even after cell death through fixation with paraformaldehyde. Swimming cells tend to aggregate massively around air bubbles trapped between the slide and the cover slip, touching them with their apex (Supplementary Material Video 7), this trait possibly caused by surface tension attraction. The mitochondria, visualized by staining their DNA with DAPI, appear as peripheral flattened tubes, which occupy a substantial part of the cell subsurface. The DNA is arranged as oval-shaped bodies, separate or fused into a network (Fig. 3A) possibly outlining the shape of the organelle. The nucleus is round and anteriorly located.

Artemidia motanka (YPF 1610) gen. n., sp. n.

The species is morphologically very similar to *N. karyoxenos* with an almost identical asymmetric structure of the apex (Fig. 2A, B), somewhat more pronounced groove extending almost half of the cell body (Fig. 2C), which is deeper in its apical part (Fig. 2C), long papilla (Fig. 2D; Supplementary Material Video 8) and subequal flagella inserted sub-apically (Fig. 2A, E, G). The cells are morphologically diverse, with the batch culture being composed of cylindrical elongated cells of variable sizes, with scattered small vacuoles and typically a larger posterior one (Fig. 2A, F). Less commonly, teardrop or pear-shaped cells with a conspicuous vacuole in the posterior part are also present (Fig. 2E, G). The cells measure 11.5 to 26.4 μm in length (19.5 ± 3 μm) and 3.9 to 8 μm in width

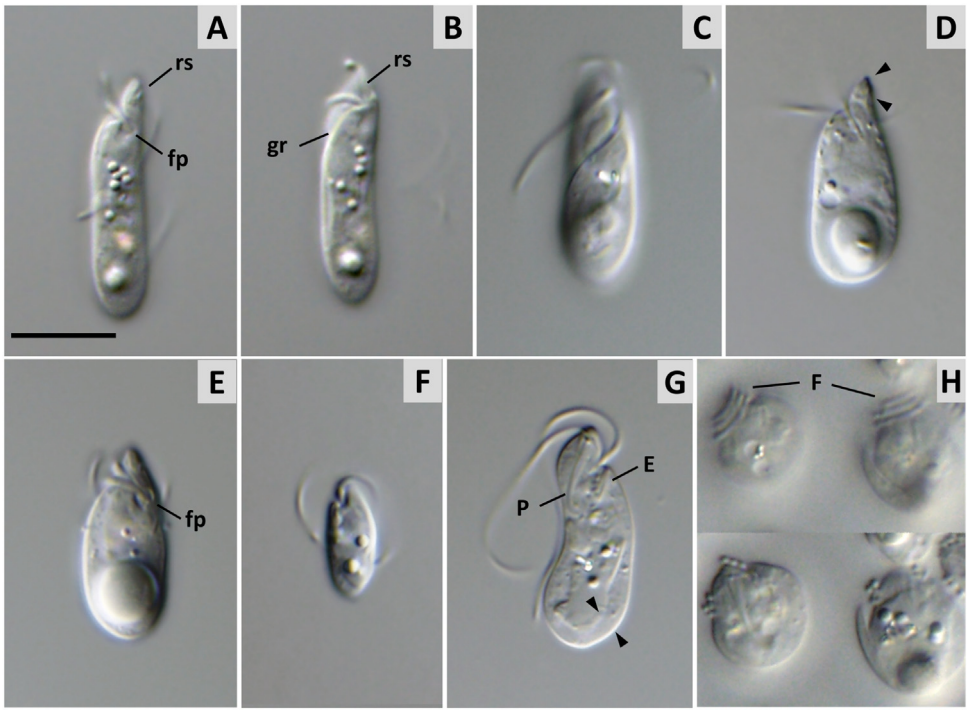

Figure 2. Differential interference contrast micrographs of *Artemidia motanka* YPF 1610, n. gen., n. sp. cultured in artificial seawater medium. (**A–C**) Cylindrical swimming cell with asymmetric anterior showing rostrum-like apex (rs), flagellar pocket (fp), and spiral groove (gr) that extends halfway down the cell. (**D**) Cell with pronounced apical papilla (between arrowheads). (**E**) Rounded cell carrying large posterior vacuole and showing lateral flagella insertion (fp). (**F**) Small cell. (**G**) Compressed cell with swollen lacunae (between arrowheads) displaying cytopharynx (P) and extrusomes (E). (**H**) Spherical sessile cells with flagella (F) wrapped around cell apex. Scale bar: 10 μm.

(5.9 ± 1.1 μm; n = 40). Spherical sessile cells with coiled flagella are also often seen at any age of the batch cultures (Fig. 2H). The metabolic and apex movements (Supplementary Material Video 9), swimming pattern and crowding behavior are similar for both species (Supplementary Material Video 10). The content of the lacunae as well as posterior vacuoles are occasionally expelled from the cells in a dramatic event (Supplementary Material Video 11). When observed under light microscope (Fig. 2G) or during fixation, the peripheral lacunae often tend to enlarge. When cells are compressed between a slide and a coverslip, the J-shaped cytopharynx and extrusomes can be clearly seen (Fig. 2G). The mitochondrion is flattened and peripheral (Fig. 3B), frequently forming a network (Fig. 3C); the nucleus is located in the anterior half of the cell. Unlike *N. karyoxenos*, *A. motanka* cannot be cryopreserved.

Cell Motility

Under optimal cultivation conditions, cells of both species are very rapid swimmers. They exhibit curvilinear runs (Supplementary Material Videos 3 and 4) interrupted by short stops or tumbles to alter their direction. During swimming in a straight path, cells cover a relatively long distance due to the high velocity. The average swimming speed of *A. motanka* is 147 μm/s (n = 15), whereas *N. karyoxenos* swims at 233 μm/s (n = 33), though some individuals can accelerate up to 500 μm/s. At an abrupt change of direction, the overall swimming speed dramatically reduces.

As they swim, cells of both species typically undergo rotation around their longitudinal axis, which is an additional way to regulate the trajectory. Their motility is mediated by the ventral and dorsal heterodynamic flagella that produce asynchronous beats at slightly different frequencies. The dorsal flagellum normally initiates a new bend first, then the ventral one follows. In *A. motanka*, the dorsal and ventral flagella beat waves at 70 Hz and 68 Hz, respectively, while for *N. karyoxenos*, the beating frequencies are 73 Hz and 80 Hz. In both flagella, waves originate at their base (Fig. 4) and then propagate till the tip at different speeds. Wave velocities

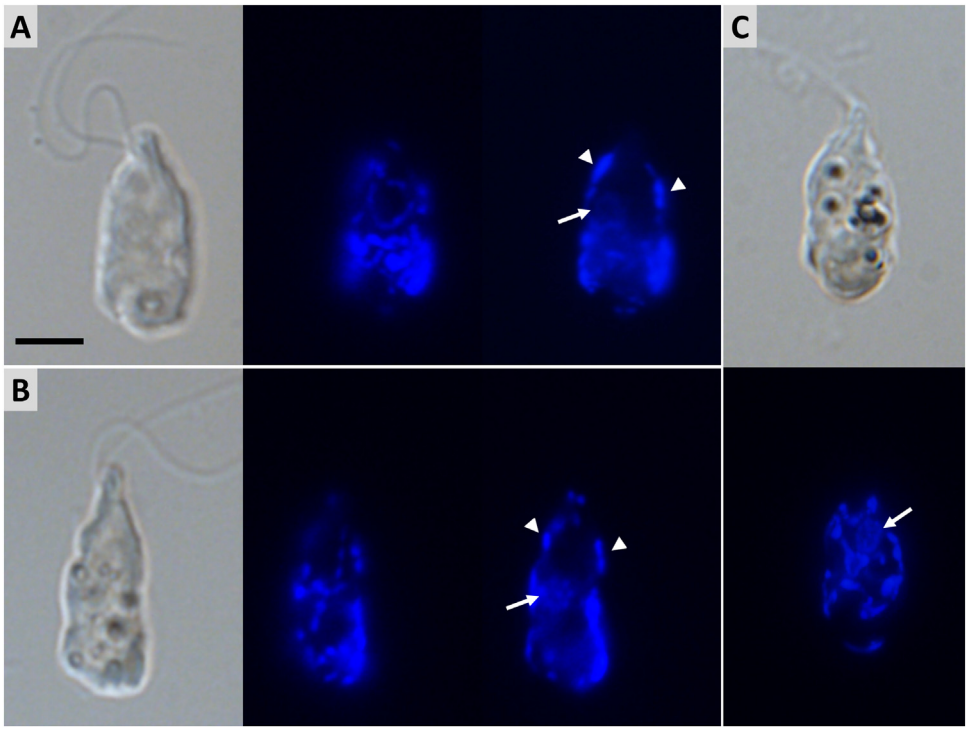

Figure 3. DAPI-stained cells of *N. karyoxenos* (**A**) and *A. motanka* (**B**) focused on cell surface (*middle*) and through nucleus (*right*). Six overlaid micrographs of DAPI-stained *A. motanka* cell showing mitochondrial network (**C**, *bottom*). Thin peripheral mitochondrial elements are marked with *arrowheads*; *arrows* point to nucleus. Scale bar: 10 μm.

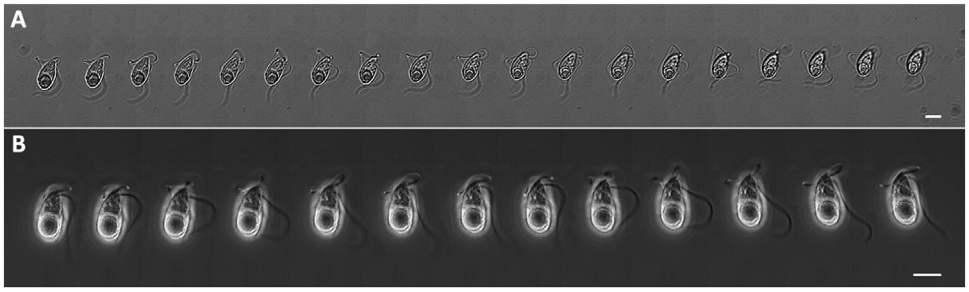

Figure 4. Waves propagation of dorsal (**A**) and ventral (**B**) flagella in *Namystynia karyoxenos*. Successive images are every 1.5 ms (**A**) and 1 ms (**B**). Scale bar: 10 μm.

of the dorsal and ventral flagella of *A. motanka* are 494 μm/s and 629 μm/s, respectively, while the values for *N. karyoxenos* are 693 μm/s and 946 μm/s. Typically, waves of both flagella are highly asymmetrical in shape with a principal bend being higher in amplitude and shorter in length than the reverse bend. The principal and reverse bends of the dorsal flagellum of *A. motanka* reach 3.7 ± 0.6 μm and 1.6 ± 0.5 μm in amplitude, and 6.5 ± 1.4 μm and 9 ± 1 μm in length, respectively. In *N. karyoxenos*, the principal bend of the dorsal flagellum is also sharp, showing 4.1 ± 1 μm in amplitude and 6.4 ± 1 μm in length, while the reverse bend is 1.8 ± 0.4 μm high and 11.6 ± 1.3 μm long.

Each subsequent principal bend of the dorsal flagellum arises in a new direction, while the previous one keeps propelling in its own orientation. Moreover, the bends may tilt during propagation. Thus, the flagellum appears as a lasso, rotating around the cell's anterior end. The ventral flagellum trails along the cell body and, as a rule, exhibits a single large principal bend followed by a reverse bend, i.e. one full wave per flagellar length. The amplitude of the principal bend of *A. motanka* is 5.3 ± 0.6 μm and the length is 10.8 ± 1.4 μm, while

for the reverse bend, these values are 2 ± 0.7 μm and 11.7 ± 1.3 μm, respectively. In *N. karyoxenos*, the ventral flagellum presents the principal bend with the amplitude of 5.7 ± 0.8 μm and length of 13.4 ± 1.8 μm, and the subsequent reverse being 2.1 ± 0.5 μm high and 15 ± 0.9 μm long. Rotation rate of the ventral flagellum is lower as compared to the dorsal one and propagation of bends along it appears to occur in one plane, so it is not twisted. Normally, a new principal bend would not appear until the previous one faded at the flagellar tip. Besides locomotion, cells use the ventral flagellum to explore and cling to surfaces. Flagellar rotation and strong asymmetries in their wave patterns result in cell oscillation during propulsion with the cell waddling from side to side (Supplementary Material Video 4).

When swimming runs are interrupted by tumbles and cell turns, both flagella demonstrate fast shaking. They produce waves at low amplitudes and large length that propagate at a higher speed. In the dorsal flagellum. these waves fade before achieving its middle part, but each successive bend gradually increases in amplitude and spreads further until, finally, one large wave covers the entire flagellum. Unlike in the dorsal flagellum, the waves of the ventral one not only reach its very tip, but slightly increase in size on their way. This behavior continues until a sudden rise of the principal bend with high amplitude and low length occurs, which efficiently pushes the cell. To perform a backward movement of the cell, both flagella produce large identical waves in the same plane followed by short smaller waves at the flagellar bases.

Ultrastructural Features

The swimming cells are characterized by smooth elongated to cylindrical shapes (Figs 5A–B, 8A). Their anterior end is characterized by the presence of a distinct apical papilla (Figs 5A–C, 8B–C). It is encircled by a single lip of the cytostome slightly protruding above the cell surface (Figs 5A–C, 8B–C). The subapical flagellar pocket is located 1–1.5 μm below the cytostome, which gives the apex an asymmetrical appearance (Figs 5A, C, 8A–C). Starting at the opening of the flagellar pocket, a longitudinal groove lines the cell body following a spiral path of about one turn (Figs 5B, 8A).

The general ultrastructure of both species is for the most part consistent with other diplonemids (Figs 5D–F, 8D). Cells are bound by a membrane with a layer of fuzzy glycocalyx on its outside (Figs 5E–G, 8D–F). The body shape is supported by a single row of parallel submembrane microtubules linked to one another by short fine filaments (Figs 5G, 8F). Evenly spaced, they encircle the cell to its posterior end along a helical path (Figs 5A, 6A–C). Most cytoskeletal microtubules abut to the membrane of the peripheral lacunae that spread almost all over the cell, occasionally forming alveolar projections (Figs 5E–G, 8D–F, 10B, F). In *N. karyoxenos*, these lacunae are normally filled with osmiophobic cubic crystals, probably containing sugars (Figs 8D–E, 10B, E–F).

Next to the lacunae, the cell's periphery is occupied by a mitochondrial network, which runs longitudinally along its length and seems to expand in the posterior half (Figs 5D, F, 8D–E, 10B, E–F). Fairly often, the mitochondrial profiles of *A. motanka* were seen extending into the middle of the cell (Fig. 5F). The organelle of this species bears only a few sparse randomly distributed lamellar cristae and numerous scattered electron-dense clots representing mtDNA (Fig. 5H–I). Mitochondrial projections of *A. motanka* resemble spheroids (Fig. 5F, H–I), which are sometimes composed of several discrete mitoplast-like lumps bound by a common membrane (Fig. 5H). Being mostly oblong in sections (Fig. 8G), the mitochondrial profiles of *N. karyoxenos* do not reach this complexity. Moreover, *N. karyoxenos* contains long lamellar cristae aligned in parallel and oriented longitudinally, as well as abundant and evenly distributed strips of electron-dense DNA in between them (Figs 8G, 10F–G).

Both species possess a relatively large nucleus, which is invariably localized in the anterior half of the cell (Figs 5D–F, 8D–E, 10B, F). Usually ellipsoidal, it is enveloped by a typical envelope with nuclear pores (Figs 5E–F, 8D–E, K, 10B–F). An electron dense, finely granular nucleolus is located either in the middle of the nucleus or slightly eccentrically (Figs 5E–F, 8D–E, 10F). In *A. motanka*, the highly condensed heterochromatin appears as a few irregular spots (Fig. 5E–F), whereas the chromatin of *N. karyoxenos* agglomerates into masses that are distributed throughout the nucleoplasm (Figs 8D–E, 10B–D, F).

The extensive Golgi complex is always adjacent to the nucleus, the proximal end of the pharyngeal lumen, and the base of the flagellar pocket (Figs 6D, J, 8K, 9D, 10E). It consists of several distinct bodies, each comprised of 12 to 23 stacked flat cisternae surrounded by lysosomal vesicles (Figs 6D, J, 8K). The posterior part of the cell is occupied by a single conspicuous digestive vacuole (Figs 5D–F, 8D–E, 10B) of variable shape and size, sometimes constituting up to 1/3 of the cell. Besides this

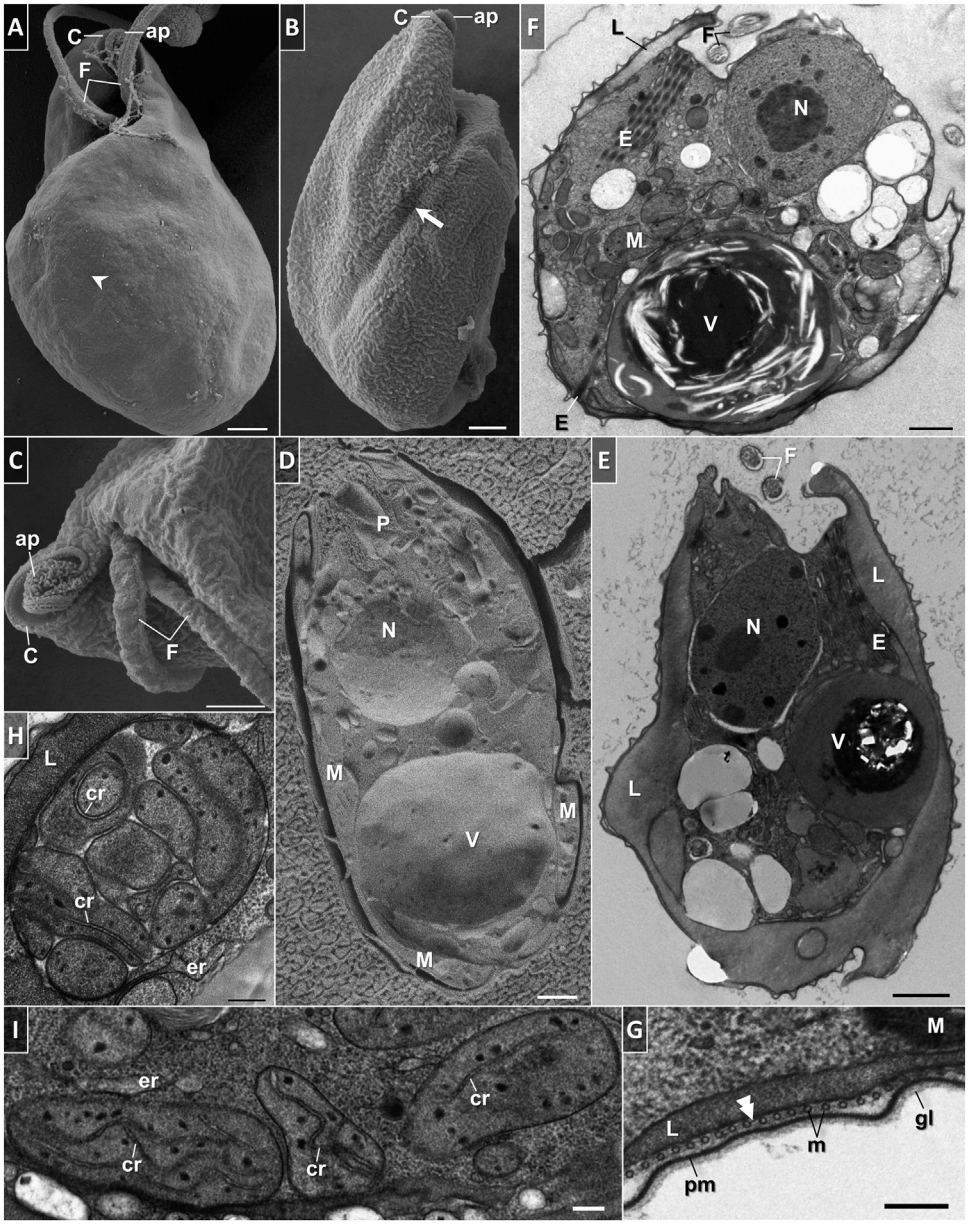

Figure 5. Micrographs showing morphology of *Artemidia motanka.* (**A–C**) General appearance of the cell with a detailed view of the apex by scanning electron microscopy. The anterior part is characterized by an apical papilla (ap) encircled with a cytostome (C), and two subapical flagella (F). The arrow points to a longitudinal groove emerging from the flagellar pocket opening. Note protruding cytoskeletal microtubules (arrowhead). **(D–E)** Freeze-fracture and transmission electron microscopy of longitudinally sectioned cell. The prominent nucleus (N), single large food vacuole (V), lacunae (L) and mitochondria (M) located at the periphery can be seen. **(F)** Oblique section through the nuclear region. Large dense nucleolus and irregular spots of peripherally located heterochromatin are present. Note the mitochondrial profiles extending in the middle of the cell, and the distribution of extrusomes (E). **(G)** Details of plasma membrane (pm) covered with glycocalyx (gl), and corset of cytoskeletal microtubules (m) interlinked by filaments (double arrowhead). **(H–I)** Sections through mitochondrial branches showing ellipsoidal profiles. The few sparse lamellar cristae (cr) and electron-dense beads of DNA are distributed randomly. Mitochondria may form mitoplast-like lumps bound by a common membrane (**H**). The cytoplasm is filled with vacuoles, vesicles, reserve granules, free ribosomes, and rare tubules of the endoplasmic reticulum (er). P – cytopharynx. Scale bars: 1 μm **(A–F)**, and 0.2 μm **(G–I)**.

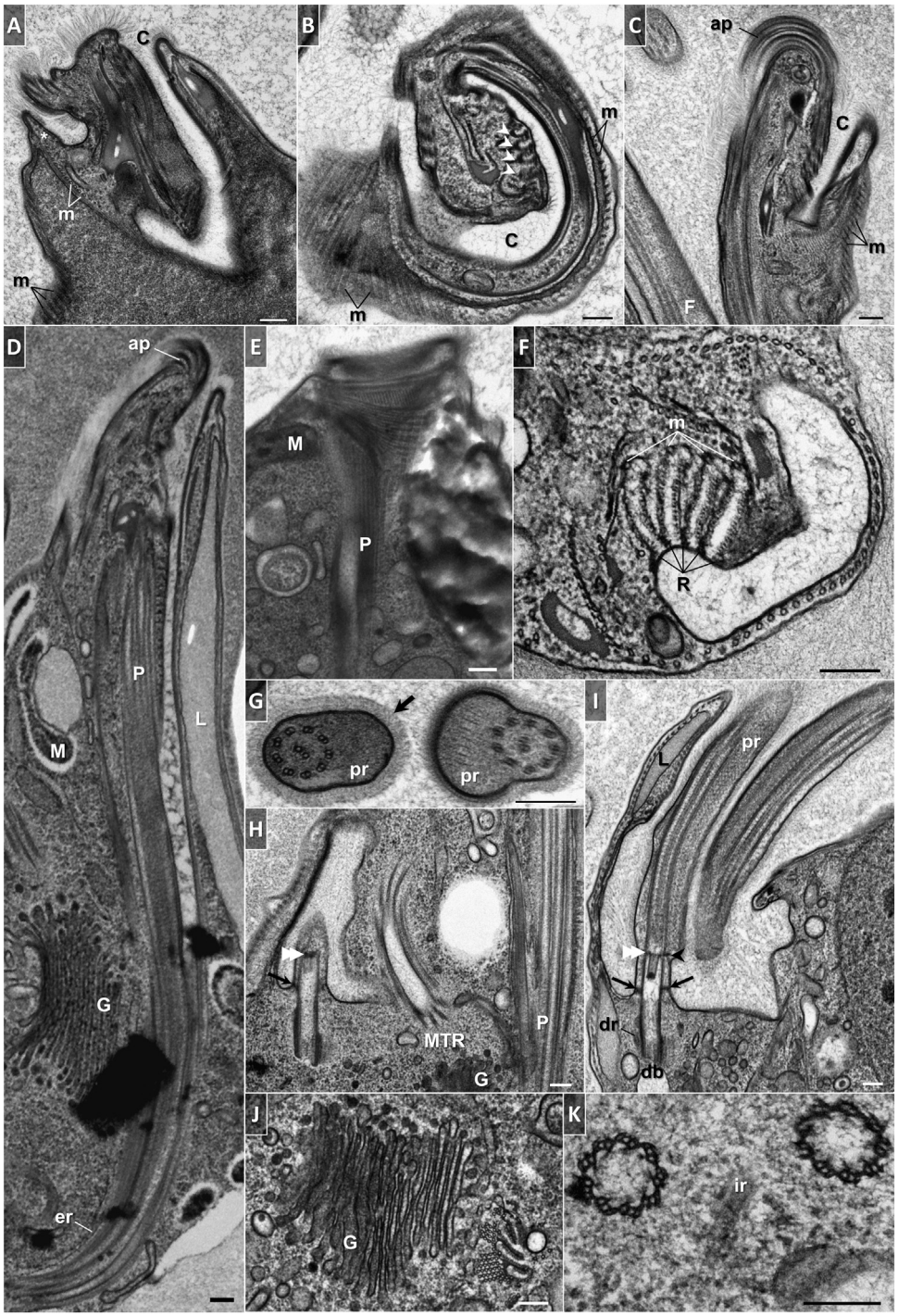

Figure 6. Transmission electron micrographs of *Artemidia motanka*. Tangential **(A)**, transverse **(B)**, and longitudinal **(C)** sections of the anterior tip of the cell showing apical papilla (ap) and cytostome (C). Asterisk marks junction between cytoskeletal microtubules (m), which follow a helical path, and microtubules supporting the cytopharynx. The transition of reinforcing microtubules (MTR) into cytopharyngeal vanes is evident (white arrowheads). Note dense hairy coat overlaying the surface membrane of the cytostome and papilla. **(D)** The longitudinal section of a horn-like tubular cytopharynx (P). Tubules of endoplasmic reticulum (er) run along its length. **(E)** Detailed view of cytopharyngeal (P) wall showing supportive fibrils and microtubules oriented longitudinally and transversely.

massive vacuole, the cytoplasm contains numerous smaller membrane-bound structures, reserve granules, free ribosomes, and sparse tubules of the endoplasmic reticulum distributed throughout the peripheral region and around the cytopharynx (Figs 5D–I, 6D–E, 8D–E, I–K).

The complex feeding apparatus has similar morphology in both species, and in the longitudinal profile appears like a horn-like tubular structure (Figs 6D, 8I). The cytopharynx is assembled from parallel ribs that are filamentous projections from four separate microtubules embedded in a fibrous material (Figs 6B, F, 8H, J). In transverse sections through the cytostome-cytopharynx region, these projections appear as U-like petals with microtubules deep at their crest (Figs 6B, F, 8H, J). A group of fibrils and tightly packed microtubules oriented longitudinally and transversely reinforce the assemblage of ribs (Figs 6B, E–F, 8H–J) that is also supported by a large semi-circular row of longitudinally oriented microtubules that lines the opposite wall of the cytopharynx (Figs 6B, F, 8J). In more posterior regions of the feeding apparatus, the cytopharynx tapers and a part of the supporting microtubules gradually terminate, the rest forms clusters that are closely associated with the microtubules at the crest of the petals (Figs 6J, 8K). The bottom of the cytopharynx is often surrounded by numerous pinocytic vesicles at early stage of formation. The surface of the cell's anterior extremity, including the cytostome, papilla, and flagellar pocket with both flagella, is typically covered by a dense hairy coat (Figs 6A–E, G, I, 8I, 9F–G).

The quartet of microtubules at the base of the cytopharynx is derived from a complex of reinforcing microtubules (MTR) that emanate from a J-like extension beneath the basal bodies at the bottom of the flagellar pocket (Figs 6H, 9F). After disbanding from the rest of the microtubules of complex, these microtubules become surrounded by a dense matrix, and while projecting toward the feeding apparatus, they form an apical papilla (Figs 6B–D, 8H). The MTR supports both the cytopharynx and the flagellar pocket and also seems to contribute to cell division. As shown in a transverse section through the flagellar pocket containing two bands of MTR, one of them is directed toward the nucleus (Fig. 9A). The emergence of a second set of MTR is most likely one of the earliest event in the replication of the flagellar pocket. Indeed, at the beginning of the cell division, the newly separated flagellar pockets already bear a characteristic single MTR per structure (Fig. 9B–C).

The rather deep flagellar pocket embraces two morphologically similar flagella – ventral and dorsal – that arise from the basal bodies located parallel and close to each other at the bottom of the pocket (Figs 6H–I, 9C, F). Both basal bodies have classical centriolar construction with slightly twisted triplet microtubules (Figs 6K, 9D). They are interconnected by fibrous material and supported by bands of three asymmetric microtubular roots (Fig. 9C–D, F). Two roots, called ventral and dorsal, attach to the sides of the ventral and dorsal basal bodies, respectively, and the third, called intermediate, runs between them (Figs 6I, K, 9F). In the proximal transitional zone, 9 triplets of basal bodies are transformed into doublets that constitute a periphery of the conventional axonemal complex (Fig. 9E). Fiber strands connect these doublets to the plasma membrane (Figs 6H–I, 9C, F). The root of the central microtubular pair of flagellar axoneme is fastened to the distal transitional plate (Figs 6H–I, 9C, F). At about the same level, the axonemes of both flagella become accompanied by a prominent paraflagellar rod of lattice-like structure, which originates from a neighboring plate and extends

(F) The cytopharynx in cross-section represented by a quartet of reinforcing microtubules (m) embedded in fibrous material and five fibrillar ribs (R). Note large semi-circular row of microtubules on the opposite wall of the cytopharynx, and bundles of supportive fibrils and microtubules. **(G)** Cross-sectioned flagella showing a 9 + 2 pattern of axonemal microtubules, paraflagellar rod (pr), and fine hairs (black arrow). **(H)** Section displaying the flagellar pocket and MTR extension emerging beneath it. **(I)** Longitudinal section of flagellar attachment zone showing relatively deep flagellar pocket. Dorsal root (dr) is seen attached to the side of the dorsal basal body (db). White double arrowheads point to the distal transitional plate. Small black arrows indicate strands of connective fibers between peripheral doublets and the plasma membrane. Note the longitudinal view of lattice-like paraflagellar rod (pr) that arise from a plate (black arrowhead) near the distal plate. **(J)** Cross-section through the feeding apparatus near the proximal end. The supportive microtubules have decreased in number and become closely associated with the quartet of reinforcing microtubules. Golgi apparatus (G) with numerous vesicles and stacked flat cisternae extends nearby. **(K)** Cross-section of basal body pair. Intermediate root (ir) runs between them. M – mitochondria, L – lacunae. Scale bar: 0.2 μm.

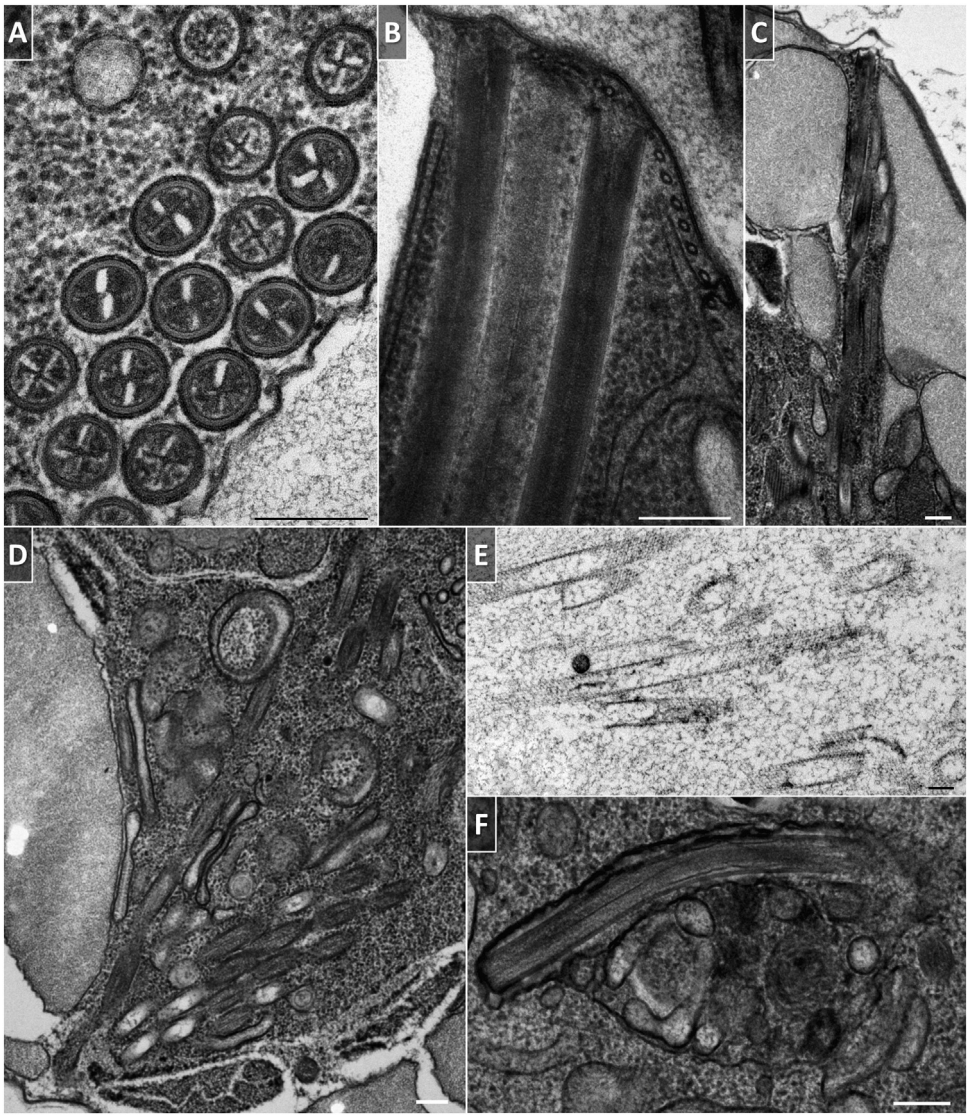

Figure 7. Transmission electron micrographs showing tubular extrusomes of *Artemidia motanka*. **(A)** Cross-section demonstrating circular profile with a cruciate center and thick double-layered wall. **(B–D)** Moment of extrusion. Note the cytoskeletal microtubules. **(E)** Lattice-like structure of discharged extrusomes. **(F)** Formation of new extrusome. Scale bar: 0.2 μm.

alongside of it almost to the tip of the flagellum (Figs 6G, I, 9C, F–G).

In *A. motanka*, a region close to the flagellar pocket is usually marked by a large accumulation of tubular extrusomes arranged in parallel (Fig. 5E–F). Additionally, batteries of extrusomes are frequently spaced along the cell's perimeter (Fig. 5F). Circular in profile, they measure 110 to 140 nm in diameter and have a cruciate center bound by electron-lucent and electron-dense layers constituting a thick wall (Fig. 7 A). Upon extrusion, they seem to push apart the cytoskeletal microtubules (Fig. 7B–C). It is unclear, though, if the discharge of several or even all extrusomes occurs through one hole or they tear the plasma membrane in a number of places (Fig. 7C–D). The ejected extrusomes appear as hollow cylinders with a lattice-like structure (Fig. 7E). Along the mature extrusomes, their nascent forms enclosed by distinct membrane systems are occasionally encountered (Fig. 7F). They are usually associated with Golgi vesicles, endoplasmic reticulum, and mitochondrion. Under standard cultivation conditions, the trophic cells of *N. karyoxenos* lack extrusomes which, however, appear upon starvation (Fig. 10E–F).

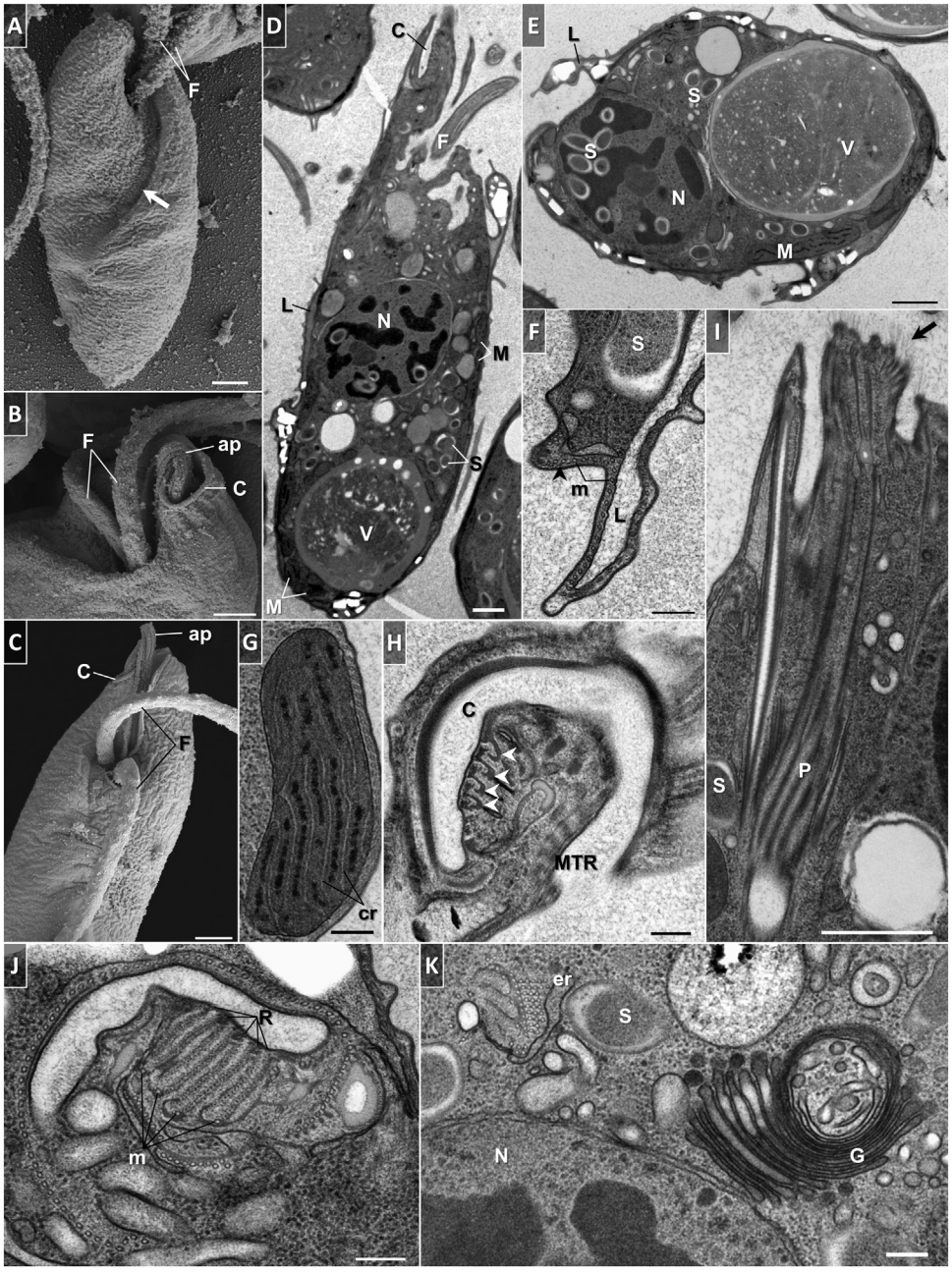

Figure 8. Scanning (**A–C**) and transmission (**D–K**) electron micrographs of *Namystynia karyoxenos.* (**A**) General appearance of the cell with the lateral longitudinal groove (white arrow) originating at the flagellar pocket opening. **(B–C)** Detailed morphology of the anterior region of the cell characterized by a cytostome (C), two subapical flagella (F), and an apical papilla (ap) in-between. **(D–E)** Longitudinal and oblique sections in the nuclear region showing principal ultrastructural organization of the cell body. The prominent nucleus (N) contains nucleolus and agglomerated masses of dense chromatin. Single large food vacuole (V) is evident in the posterior part of the cell. Peripherally positioned mitochondria (M) and lacunae (L) extensions with white cubic crystals are seen. Note the distribution of intracellular bacterial symbionts (S). **(F)** Transverse profiles of peripheral microtubules (m) interlinked by filaments (black arrowhead). Note the membranes of peripheral lacunae (L). **(G)** Sections through mitochondrial profile with its large lamellar cristae (cr) running in parallel and electron-dense DNA in-between. **(H)** Transverse sections through the cell anterior showing cytostome (C) and band of reinforcing microtubules (MTR) transiting into cytopharyngeal vanes (white arrowheads).

The nucleus and cytoplasm of *N. karyoxenos* are packed with rod-shaped endosymbiotic bacteria (Figs 8D–F, I, K, 9C, 10B–D, F). They are enveloped by double membranes with a periplasmic space and comprise an electron-dense granular inner matrix (Fig. 10A). The cytoplasmic endosymbionts are usually localized in close proximity to the mitochondrion or even seem to penetrate into it (Figs 8D–E, 10B), especially when cells are starved (Fig. 10F–G). A prominent feature of bacteria localized within the nucleus is that they are surrounded by heterochromatin (Figs 6D–E, 10B–D, F). Bacterial division occurs via a constriction in the middle of the cell (Fig. 10D). No signs of lysis or degradation of the endosymbionts have been observed.

Molecular Phylogeny

Both *Artemidia motanka* gen. n., sp. n. and *Namystynia karyoxenos* gen. n., sp. n. branch within Diplonemea and more specifically, within Hemistasiidae with robust support (Fig. 11). Given the rather divergent nature of their 18S rRNA gene sequences (Fig. 11), we tested their affiliation to Hemistasiidae using AU tests and were able to reject all the alternative topologies with *A. motanka* and *N. karyoxenos* as members of all remaining diplonemid clades (Eupelagonemidae, DSPD II and Diplonemidae). The 18S rRNA gene sequences of novel strains show that they are clearly different from the hemistasiid type species *H. phaeocysticola*. The graphic representation (Fig. 11; see branch lengths) as well as the more exact percentage of base differences (21% divergence for *N. karyoxenos*-to-*H. phaeocysticola* and 17% for *A. motanka*-to-*H. phaeocysticola* and 19% for *N. karyoxenos*-to-*A. motanka*) justify the placement of both species into newly established genera.

Molecular phylogenetic position of endosymbiont. The maximum likelihood 16S rRNA gene phylogeny of the novel endosymbiont of *N. karyoxenos* places it within the α-proteobacterial order Rickettsiales (Fig. 12), where we have established a new genus "*Candidatus* Sneabacter" to accommodate "*Ca.* Sneabacter namystus" sp. nov. Rickettsiales are split into three well-supported clades. First one contains specimens of *Ehrlichia*, *Wolbachia*, *Anaplasma* and *Neorickettsia*, while the second clade comprises of several endosymbionts of ciliates and amoebae including *Midichloria*, *Cyrtobacter*, *Lyticum* and several environmental/uncultured sequences. Finally, within the third clade, the suggested *Candidatus* Sneabacter namystus forms a sister branch to another endosymbiont derived from the ciliate *Pseudomicrothorax dubius*. They branch as a sister group to the *Rickettsia* species, including several endosymbionts of protists, excluding the Orientia/Occidentia clade. Since other bacterial endosymbionts recently described from the diplonemids *Diplonema japonicum* and *D. aggregatum* are members of the α-proteobacterial clade *Holosporales* (Tashyreva et al. 2018b), we have also tested the possibility that the suggested *Ca.* Sneabacter namystus has an affinity to *Holosporales*. The AU test clearly rejects this alternative hypothesis and thus confirms the assignment of *Ca.* Sneabacter namystus to the Rickettsiales.

Discussion

We describe two new species of diplonemids in order to better understand the morphology, diversity, life style and ecological significance of this elusive group of protists, likely composed of tens of thousands of species (David and Archibald 2016; Flegontova et al. 2016; Gawryluk et al. 2016; Okamoto et al. 2019). Until now, less than a dozen of diplonemids and only a single hemistasiid have been formally described (Tashyreva et al. 2018b), the main obstacle being their inconspicuous morphology and a failure to grow under laboratory conditions.

Both species robustly fall into the recently established family Hemistasiidae (Cavalier-Smith 2016), and each clearly represents a separate genus,

(I–J) Longitudinal and transverse sections through complex cytopharynx (P) composed of five fibrillar ribs (R) that take their origin from a quartet of reinforcing microtubules (m) embedded in fibrous material, accompanied by large semi-circular row of microtubules on the opposite wall, and bundles of supportive fibrils and microtubules along its entire length. Black arrow points to the dense lush hairy coat overlaying the surface membrane of the cytostome. **(K)** Section indicating relative placement of the posterior region of the cytopharynx, nucleus (N), and Golgi complex (G). The cytopharynx is surrounded by tubules of endoplasmic reticulum (er) and vesicles. The cytoplasm is filled with vacuoles, reserve granules, and free ribosomes. Scale bars: 1 μm **(A–D)**, and 0.2 μm **(E–K)**.

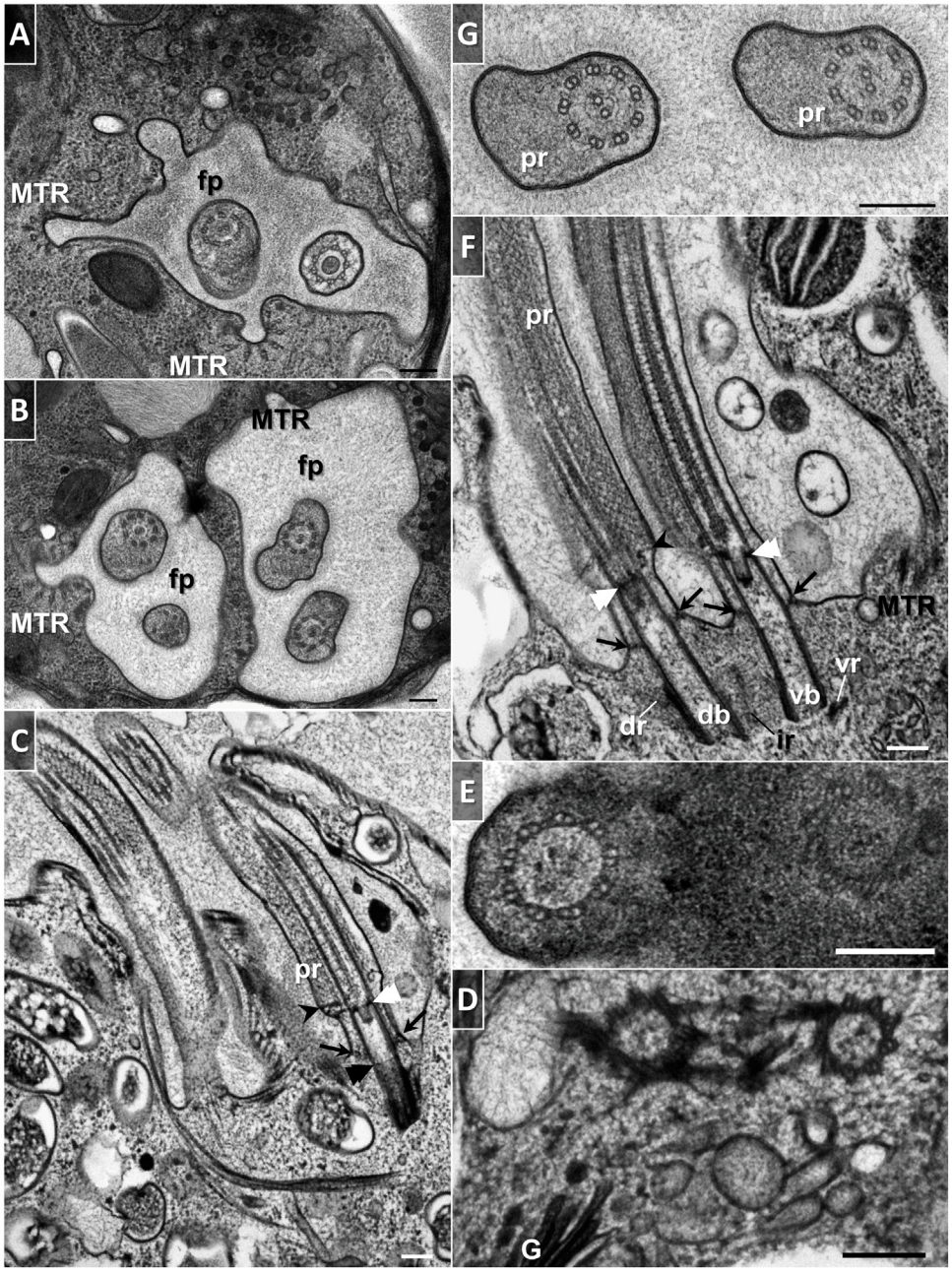

Figure 9. Transmission electron micrographs of the flagellar apparatus of *Namystynia karyoxenos*. Selected transverse (**A–B**) and longitudinal (**C**) sections of the flagellar pocket (fp) undergoing replication. In early phase of events, the microtubule-reinforced region (MTR) is apparently duplicating first. Distal and proximal transitional plates are indicated by white and black double arrowheads, respectively. (**D**) Detail of basal bodies centriolar configuration. Connective fibers and Golgi complex (G) are evident. (**E**) Oblique section through the transitional zone showing nine microtubule doublets. (**F**) Longitudinal section in region of flagellar attachment illustrating ventral (vb) and dorsal (db) basal bodies arranged parallel to each other, with ventral (vr) and dorsal (dr) roots attached to their sides, and intermediate root (ir) in-between. Black arrows point to the strands of connective fibers between peripheral doublets and the plasma membrane. Arrowheads indicate origin of paraflagellar rod (pr). (**G**) Cross-section of the free flagella having typical axoneme with the adjacent conspicuous paraflagellar rod (pr), and fine hairs. Scale bar: 0.2 μm.

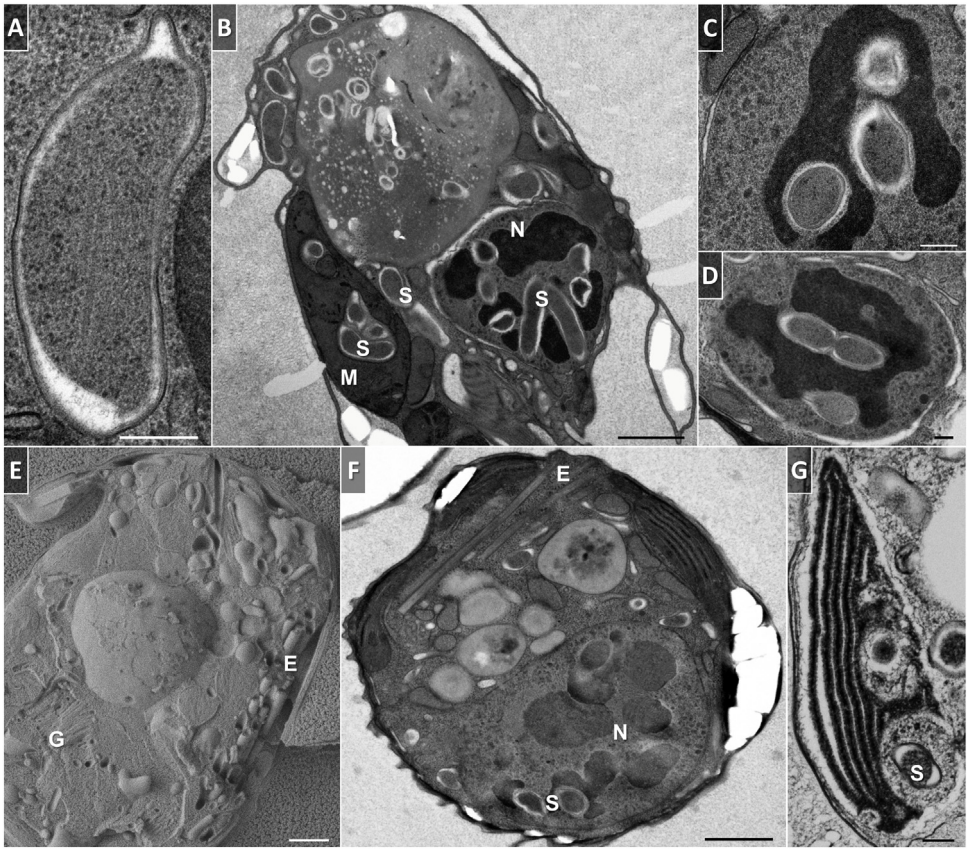

Figure 10. Electron micrographs showing intracellular bacteria and extrusomes in *Namystynia karyoxenos*. (**A**) Detail of the rod-shaped endosymbiotic bacterium with double membrane, prominent periplasmic space, and granular interior. (**B**) A cell with endosymbionts (S) concentrated in the cytoplasm, nucleus (N), and near the mitochondrial profiles (M). (**C–D**) Intranuclear bacteria surrounded by a heterochromatin. Bacterial division occurs via a constriction in the middle of the cell. Freeze-fracture (**E**) and transmission (**F**) electron microscopy of starving cells showing tubular extrusomes (E) and Golgi complex (G). (**G**) The mitochondria of cell under starving conditions are seen to enclose the endosymbiotic bacteria. Scale bars: 0.2 μm **(A, C–D, G)**, and 1 μm **(B, E–F)**.

established on the basis of significantly different 18S rRNA genes, as well as distinct ultrastructural features. *A. motanka* and *N. karyoxenos* are indistinguishable from each other at the level of light microscopy, as they have similar dimensions, and no discrete distinguishing features. However, extremely close resemblance of diplonemids belonging to different species or distant genera has been noted before (Tashyreva et al. 2018a). The present study once again reveals significant limits of their taxonomy, as long as it is based exclusively on light microscopy, in the absence of any ultrastructural and molecular data (Larsen and Patterson 1990; Tashyreva et al. 2018a, 2018b; von der Heyden et al. 2004). This particularly concerns a number of 'hemistasiid-like' protists, for which only very limited descriptions are available (Schiller 1925; Throndsen 1969; Vørs 1992). It is hard to exclude the possibility that *A. motanka* and *N. karyoxenos* are identical to one or other these previously described species, for example *Entomosigma peridinioides* (Schiller 1925) or *Cryptaulax marina* (von der Heyden et al. 2004; Throndsen 1969), which share cell shape, flexibility, and having a rostrum and a spiral groove with our species, but without the morphological and ultrastructural evidence it is difficult to confirm.

In the exponentially growing cultures, both species exhibit a range of morphologies with extensive size, shape and cytoplasmic content variability, so we anticipate an even more pronounced morphological diversity in their natural environment. A similar polymorphism, with individual cells progressing through the cycle in an asynchronous manner was observed in *H. phaeocysticola* (Elbrächter et al. 1996). However, this

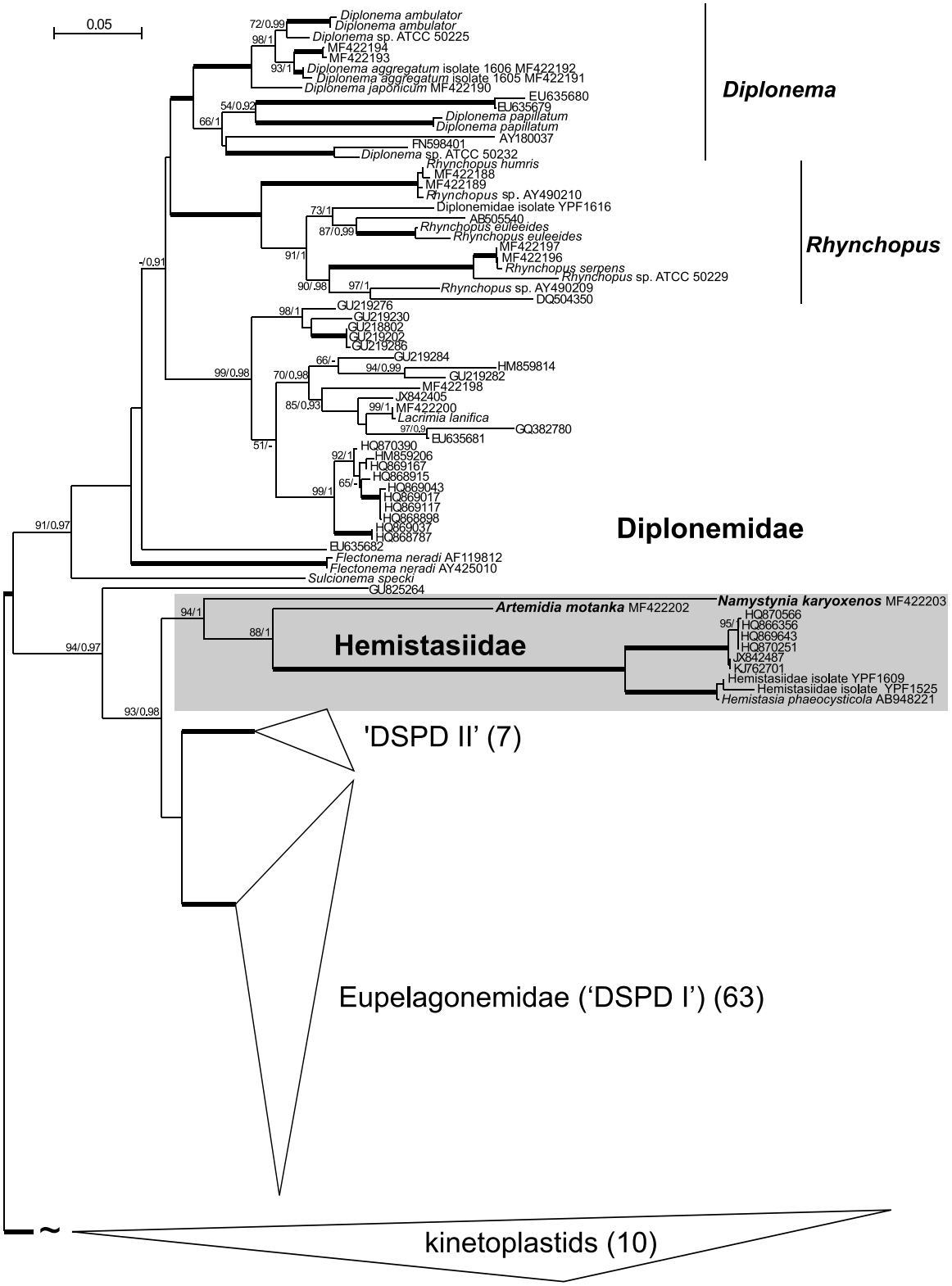

Figure 11. Phylogenetic position of *Namystinia karyoxenos* and *Artemidia motanka* as revealed by maximum likelihood analysis of 18S rDNA dataset of Diplonemida. Newly described taxa are highlighted in bold font. Thick branches represent absolute support (i.e. bootstrap values of 100 and Bayesian posterior probabilities of 1.0). Tree is adopted from Tashyreva et al. 2018a.


0.05
bacterial symbiont of Diophrys sp. AJ630204
Rickettsiaceae endosymbiont of Pleodorina japonica AB688629
EF667896
CU466797
HQ691997
Rickettsia sp. WE2 HE648946
Rickettsia sp. WE1 HE648945
endosymbiont of Haplosporidium sp. AJ319724
FJ203077
Rickettsia endosymbiont of Nuclearia pattersoni AY364636
Rickettsia endosymbiont of Torix tagoi AB066351
Rickettsia rickettsii L36217
Rickettsia japonica NR_074459
Rickettsia prowazekii M21789
Rickettsia bellii L36103
Rickettsiales (46)
Ca. Sneabacter namystus symbiont of Namystynia karyoxenos
Ca. Cryptoprodotis polytropus FM201293
Orientia chuto NR_117903
Rickettsia tsutsugamushi U17258
Orientia tsutsugamushi NR_025860
Occidentia massiliensis GU937608
GQ347698
Ca. Anadelfobacter veles host Euplotes harpa FN552695
Ca. Cyrtobacter zanobii HE978250
EU555284
Ca. Midichloria mitochondrii AJ566640
Rickettsiales endosymbiont of Nysius plebeius AB624350
JQ337869
EF667901
EU394580
FJ437943
Ca. Defluviella procrastinata HE978248
Lyticum flagellatum NR_125566
Lyticum sinuosum HF969038
EU236349
endosymbiont of Acanthamoeba sp. UWC8 AF069963
Wolbachia pipientis X61768
Anaplasma phagocytophilum NR_044762
Anaplasma odocoilei NR_118489
Ehrlichia bovis U03775
Ca. Neoehrlichia mikurensis AB196304
Ehrlichia chaffeensis NR_037059
Ehrlichia canis M73221
Neorickettsia helminthoeca U12457
Ehrlichia risticii M21290
Neorickettsia sennetsu NR_074386
Holosporales (47)
Rhodobacterales (11)
Rhizobiales (24)
Rhodospirillales (9)
Magnetococcus marinus NR_074371

species differs from *A. motanka* and *N. karyoxenos* by the absence of glycocalyx and a spiral groove (Elbrächter et al. 1996), the latter being subject of numerous debates (Al-Qassab et al. 2002; Bernard et al. 2000; Elbrächter et al. 1996; Griessmann 1913; Lee 2015). By examining slow motion video sequences, Elbrächter et al. (1996) claimed that the previously reported groove of *H. phaeocysticola* is an artefact caused by flagellar beating. While hard to distinguish by light microscopy, this character should not be missed by scanning electron microscopy, however, to our knowledge no images by this technique are available for *H. phaeocysticola*. From all diplonemids described so far, the existence of a curved furrow has been convincingly shown only for *Flectonema neradi* (Tashyreva et al. 2018a).

The apex of *H. phaeocysticola* consists of a flexible rostrum (Elbrächter et al. 1996). We adopted this term to describe the protruding apical part of *A. motanka* and *N. karyoxenos*, although their apexes are broader and less pointy. Diplonemids are generally characterized by an asymmetrical anterior region of the cells, a feature defined by the sub-apical flagellar pocket (Porter 1973; Schuster et al. 1968; Tashyreva et al. 2018a,b; Triemer and Ott 1990). It should be mentioned, however, that in hemistasiids, the flagellar pocket has a significantly more posterior location than in members of Diplonemidae.

For the most part, both species described here demonstrate ultrastructural similarities that are consistent with the cellular organization of other diplonemids (Roy et al. 2007; Schnepf 1994; Triemer and Ott 1990). A set of features that unify most diplonemids include a highly complex feeding apparatus with a papilla, a well-developed metaboly, and a highly reticulated peripheral mitochondrion packed with DNA bundles (Porter 1973; Tashyreva et al. 2018a,b; Triemer and Ott 1990). At the same time, Hemistasiidae distinguish themselves from other Diplonemea by the presence of a combination of peripheral lacunae, batteries of extrusomes, a large posterior vacuole and permanent paraflagellar rods in both flagella that allow a fast and complex swimming pattern. Still, at present only lacunae can serve as an apomorphy of Hemistasiidae, since the remaining traits also appear in at least some life cycle stages of other diplonemids (Tashyreva et al. 2018a,b). Consequently, we agree with Cavalier-Smith (2016) that *Phyllomitus amylophagus* (Mylnikov et al. 1998) does not belong to the hemistasiids. This protist not only lacks the peripheral lacunae and possesses a nemadesm (a single microtubular rod lying alongside the feeding apparatus, common in kinetoplastids), but also exhibits numerous discoidal cristae and much simplified feeding apparatus. The role of the lacunae remains to be elucidated, however, taking into account their swelling during fixation (Elbrächter et al. 1996; Scherffel 1900; this study), they might be responsible for osmoregulation. We noticed a peculiar behavior during which the content of lacunae, as well as that of the food vacuole was expelled "en block" from the cell. Similar ability has also been observed in the eupelagonemid diplonemids (N. Okamoto and P.J. Keeling, personal communication). Most diplonemids carry several food vacuoles (Tashyreva et al. 2018a,b; Triemer and Ott 1990), although species with only a single digestion vacuole were also reported (Porter 1973; Schuster et al. 1968; Tashyreva et al. 2018a).

The ultrastructural features that discriminate *A. motanka* from *N. karyoxenos* include the uneven pattern of mitochondrial lumen, the invariable presence of tubular extrusomes, the absence of endosymbionts and the abundance of cubic crystals within lacunae in the former species. In contrast to *N. karyoxenos*, the nucleus of *A. motanka* closely resembles that of *H. phaeocysticola* (Elbrächter et al. 1996) in having only a few irregular spots of heterochromatin, an unusual feature for diplonemids (Porter 1973; Tashyreva et al. 2018a,b; Triemer 1992). In addition, only *N. karyoxenos* can be cryopreserved, which likely reflects its ultrastructural and biochemical characters.

The most striking structural alterations concern the mitochondria of *N. karyoxenos*, as this

Figure 12. Maximum likelihood topology of 16S rDNA dataset of alpha proteobacteria showing phylogenetic position of novel hemitasiid symbiont *Candidatus* Sneabacter namystus (highlighted in bold). The tree was estimated in IQ-Tree under the Tranversional model with equal base frequencies and six relaxed categories of variable sites (TVMe + R6). Branching support was estimated using thorough non-parametric bootstrap algorithm as implemented in IQ-Tree from 1000 replicates as well as Bayesian posterior probabilities estimated by PhyloBayes 4 under the C20 + GTR model. Support values are represented either by bold branches (100 BS, 1.0 PP) or actual numbers for support values of 99–50%/0.99–0.9. Values below 50%/0.9 are not shown. For more details see respective part of Materials & Methods. Please note that polytomy of outgroup bacterial clades reflect lack of branching support as well as colliding maximum likelihood and Bayesian inference topologies.

species presents a highly organized lumen with DNA arranged in parallel strips. Like other diplonemids (except *F. neradi* (Tashyreva et al. 2018a)), the mitochondrion of hemistasiids is furnished with just a few very large lamellar cristae, and sometimes forms unusual structures, such as discrete mitoplast-like lumps (Elbrächter et al. 1996; this study). A unique aspect of the diplonemid mitochondria is the massive amount of DNA they contain (Lukeš et al. 2018) and the extremely complex processing of its RNA, which involves massive *trans*-splicing and several types of RNA editing (Burger and Valach 2018; Valach et al. 2016; Yabuki et al. 2016). Moreover, in hemistasiids these features and mechanisms reach extreme levels of complexity (manuscript in preparation). The shared presence of the uridine insertion type of RNA editing in diplonemids and kinetoplastids may be inherited from their common ancestor (Flegontov et al. 2011; Kiethega et al. 2011; Marande and Burger 2007).

Ultrastructural examination of *N. karyoxenos* revealed the presence of the endosymbiont *Ca.* Sneabacter namystus, a member of Rickettsiales, which significantly extends our knowledge of endosymbiotic bacteria in diplonemids (Tashyreva et al. 2018b). This group of α-proteobacteria lacks known free-living members and are commonly found as endosymbionts or parasites in various single-celled as well as multicellular eukaryotic lineages, including humans (Szokoli et al. 2016). *Ca.* Sneabacter namystus is abundant in the cytoplasm of *N. karyoxenos* and is also non-randomly positioned adjacent to the mitochondrion, occasionally even penetrating into it. In addition, they were found to also colonize the nucleus and multiply therein, first case of this kind in diplonemids. However, it should be noted that such symbiotic relationship between α-proteobacteria and ciliates or amoebae is fairly common (Schulz and Horn 2015), although the role(s) of partners remain largely unknown. Thus, diplonemids may constitute a good model for the study of the energy metabolism of an endosymbiont, as well as the bacterial-host interactions.

To date, only three diplonemid species have been reported to constantly carry the tubular extrusomes (Elbrächter et al. 1996; Schuster et al. 1968; this study). They seem to be synthesized in Golgi vesicles or endoplasmic reticulum (Elbrächter et al. 1996; Hausmann 1978; this study). Even though extrusomes are frequently reported from euglenozoans (Brugerolle 1985; Mignot and Hovasse 1973; Simpson et al. 1997; Yubuki et al. 2009), their functional significance in this eukaryotic supergroup remains largely unclear. Considering the fact that in diplonemids this organelle appears in only certain life stages (Tashyreva et al. 2018b; this study), the extrusome is presumably used for defence against predators and/or to capture a prey. In contrast to *H. phaeocysticola* (Elbrächter et al. 1996), neither *A. motanka* nor *N. karyoxenos* have so far been observed to actively attack diatoms (data not shown), as they seem to prefer feeding on detritus.

Despite a wide array of possible life strategies (Elbrächter et al. 1996; Simpson 1997; Triemer and Ott 1990), all diplonemids possess a morphologically similar complex feeding apparatus, which is homologous to the feeding apparatus of kinetoplastids (Kivic and Walne 1984) and phagotrophic euglenids (Leander et al. 2007; Mignot 1966). It is assumed that the MTR pocket was present in the ancestral euglenozoan (Leander 2004), which in the diplonemid lineage evolved into a greatly embellished feeding apparatus (Montegut-Felkner and Triemer, 1996; Triemer and Farmer 1991).

Until recently, in their trophic stage diplonemids were invariably considered to bear short flagella or flagellar stubs (Roy et al. 2007; Schnepf 1994; Tashyreva et al. 2018a; Triemer 1992) that grew into long and fully motile structure in the swimming stage (Tashyreva et al. 2018b; Vickerman 2000; von der Heyden et al. 2004). Along with *Artemidia* and *Namystynia*, only the members of *Hemistasia* and *Lacrimia* carry two long flagella with permanent paraflagellar rod supporting the axoneme (Elbrächter et al. 1996; Tashyreva et al. 2018a). In contrast to several previous reports (Larsen and Patterson 1990; Porter 1973; Schuster et al. 1968), the flagella of many diplonemids are decorated with hairs reminiscent of those known from other euglenozoans (Tashyreva et al. 2018a,b). The ultrastructural features of the flagellar apparatus generally unify the euglenozoan assemblage, with one exception being the proximal transitional plate in the hollow transition zone, which is complemented by the distal plate only in diplonemids and kinetoplastids (Montegut-Felkner and Triemer 1994; Triemer and Farmer 1991).

We can only assume the range of dramatic changes in natural habitats of *A. motanka* or *N. karyoxenos*, where active or passive translocation even for a short distance would be detrimental to their swimming ability. Nevertheless, cells seem to be ideally adapted to extreme environmental conditions, as they possess a paraflagellar rod that facilitates fast motion (Hughes et al. 2012) and exhibit different motility patterns. For relocation they move rapidly in more or less straight lines, and, alternatively, cells abruptly slow down and often tumble in order to stay in a restricted area. Consid-

ering their attraction to the surfaces and changes in the flagellar beating, the latter may represent a food-seeking strategy. In its course, the two heterodynamic flagella can temporally switch their functions, with one responsible for the movement, and the other for a contact with substrate or groping. Thus, cells are able to react to rapid changes in their vicinity, and if need be, actively move into more favorable environment.

Based on molecular phylogenetics, diplonemids constitute the sister lineage of kinetoplastids, while euglenids branch basally to the two (Kiethega et al. 2011; Marande and Burger 2007; Simpson and Roger 2004). It seems, however, that the euglenids and kinetoplastids managed to retain a set of similar unique features, while often they are missed in diplonemids examined to date. The Hemistasiidae species possess all three euglenozoan synapomorphies, namely the paraflagellar rod, the asymmetric arrangement of the flagellar root system and the tubular extrusomes. This leads us to speculate that hemistasiids might be intermediate ('morphological link') between structurally divergent diplonemids and other euglenozoans. Apparently, all these distinctive features were present in a common ancestor of diplonemids, however, some of the species independently lost them since the point of divergence.

Taxonomic Summary

Phylum Euglenozoa Cavalier-Smith, 1981

Class Diplonemea Cavalier-Smith, 1993

Order Diplonemida Cavalier-Smith, 2016

Family Hemistasiidae Cavalier-Smith, 2016

Genus ***Artemidia*** gen. n. Prokopchuk, Tashyreva and Lukeš, 2019

Diagnosis. Marine hemistasiid distinguished from related genera by ultrastructural and molecular features. Cells mostly cylindrical, elongated, less commonly teardrop or pear-shaped with a conspicuous posterior vacuole; 11.5–26.4 μm in length by 3.9–8 μm in width. Rounded sessile cells with coiled flagella often seen at any age of the cultures. Spiral groove halfway down the body. Mitochondrion oblong or rounded in profile with large lamellar cristae. Tubular extrusomes of a lattice-like structure. Peripheral lacunae filled with refractive granules.

Etymology. The generic name (feminine) refers to Artemis, a Greek goddess, who carries bow and arrows, which are reminiscent of extrusomes.

Type species: *Artemidia motanka*.

Artemidia motanka sp. n. Prokopchuk, Tashyreva and Lukeš, 2019

Description. Very active, rotate and oscillate; metabolic. Highly asymmetric apex with long and flexible apical papilla and a rounded posterior end. Two long heterodynamic flagella inserted subapically, both with paraflagellar rods and flagellar hairs. Dorsal flagellum beats around cell apex, ventral trails. Nucleus in anterior half. Glycocalyx present.

Etymology. The species name is derived from Czech word 'motat' ('to coil' in English), which reflects the tendency of cells to coil their flagella around the cell's apex.

Type strain. YPF 1610

Type material. An OsO_4-fixed slide and a genomic DNA sample of YPF 1610 are deposited in the protistology collection of the Institute of Parasitology, Biology Centre, Czech Academy of Sciences, České Budějovice, № IPCAS Pro 55. This material collectively constitutes the name-bearing type (an hapantotype) of the species.

Gene sequence. MF422202, 18S rRNA gene, partial sequence

Type locality. Coastal waters of Yokosuka, Japan (latitude 35.3194°N; longitude 139.6507°E)

Phylum Euglenozoa Cavalier-Smith, 1981

Class Diplonemea Cavalier-Smith, 1993

Order Dilonemida Cavalier-Smith, 2016

Family Hemistasiidae Cavalier-Smith, 2016

Genus ***Namystynia*** gen. n. Prokopchuk, Tashyreva and Lukeš, 2019

Diagnosis. Marine hemistasiid distinguished from related genera by ultrastructural and molecular features. Trophic cells show pleomorphism, predominantly long, cylindrical with round posterior end and highly asymmetric apex, some pear-shaped carrying a large posterior vacuole, spherical sessile cells with both flagella coiled around the anterior region of the cell are frequent; 13–27 μm long and 4–8 μm wide; extrusomes absent. Starved cells short and rounded, contain extrusomes. Spiral furrow along half of the body. Peripheral mitochondria flattened, with large lamellar cristae and DNA arranged in parallel strips. Peripheral lacunae with clear matrix. Endosymbionts.

Etymology. The generic name (feminine) is inspired by pleomorphic cells, which appear as various shiny beads ("Namystyna" in Ukrainian).

Type species: *Namystynia karyoxenos*.

Namystynia karyoxenos sp. n. Prokopchuk, Tashyreva and Lukeš, 2019

Description. Cells highly metabolic; swim fast with rotation around the longitudinal axis and oscillations. Two long flagella sub-apical with paraflagellar rods and flagellar hairs, heterodynamic, dorsal loops around cell apex, ventral trails. Long and flexible apical papilla. Glycocalyx present. Nucleus central or in anterior half.

Remarks. Can be cryopreserved in liquid nitrogen.

Etymology. Latinized, the species name reflects the hosting of endosybionts by the nucleus.

Type strain. YPF 1621

Type material. An OsO_4-fixed slide and a genomic DNA sample of YPF 1621 are deposited in the protistology collection of the Institute of Parasitology, Biology Centre, Czech Academy of Sciences, České Budějovice, № IPCAS Pro 56. This material collectively constitutes the name-bearing type (an hapantotype) of the species.

Gene sequence. MF422203, 18S rRNA gene, partial sequence

Type locality. Coastal waters of Yokosuka, Japan (latitude 35.3194°N; longitude 139.6507°E)

Endosymbiont

Phylum Proteobacteria Garrity et al., 2005

Class Alphaproteobacteria Garrity et al., 2005

Sublass Rickettsidae Ferla et al., 2013

Order Rickettsiales Gieszczkiewicz, 1939

Family Rickettsiaceae Pinkerton, 1936

Genus "*Ca.* Sneabacter" gen. n. Prokopchuk, Tashyreva and Lukeš, 2019

Description. Genus of endosymbiotic bacteria distinguished from related genera by molecular phylogeny. Rod-shaped, 0.9–1.2 μm long and 0.25–0.33 μm wide, possible striated inclusions, Gram-negative cell wall organization, spores not observed. Reside freely in the cytoplasm mostly near mitochondria, which they may penetrate; within the nucleus they are surrounded by heterochromatin. Not accompanied by additional host membranes.

Etymology. The name (masculine) is attributed to the ability to sneak into the organelles of the host.

"***Ca.* Sneabacter namystus**" sp. n. Prokopchuk, Tashyreva and Lukeš, 2019

Description. Species identified by distinct position on 16S rRNA phylogenetic tree.

Etymology. The name is acquired from the host *Namystynia*.

Type host. *Namystynia karyoxenos*.

Methods

Isolation and cultivation of cells: Strains were harvested from the coastal waters at the port in JAMSTEC headquarters, Yokosuka, Japan (35.3194°N, 139.6507°E). The axenic clonal cultures were established manually by single cell isolation with a microcapillary pipet and were grown in an artificial medium composed of 3.6% sea salts (Sigma-Aldrich), 1% (v/v) heat-inactivated horse serum (Sigma-Aldrich), 0.025 g/l LB broth powder (Amresco), supplemented with 10 μl/ml antibiotic cocktail (P4083, Sigma-Aldrich). The medium was sterilized by filtration via a 0.22 μm Millipore filter. The cultivation was performed in plastic tissue culture flasks containing antibiotic-free medium at 22 °C under a 12 h light/12 h dark cycle.

DNA isolation, sequencing and phylogenetic analysis: Total genomic DNA was isolated using the DNeasy Blood & Tissue Kit (Qiagen) following the protocol A. The nearly full-size 18S rRNA gene was amplified with universal eukaryotic primers SA (5′-AACCTGGTTGATCCTGCCAGT-3′) and SB (5′-TGATCCTCCTGCAGGTTCACCT-3′) and sequenced. A partial 16S rRNA gene sequence from the endosymbiont was amplified with bacteria-specific forward (5′-GCTTAACACATGCAAG-3′) and reverse primers (5′-CCATTGTAGCACGTGT-3′) yielding 1180 bp-long amplicons.

18S rRNA phylogeny of *Artemidia motanka* gen. n., sp. n. (labeled by its original strain number YPF1610), and *Namystynia karyoxenos* gen. n., sp. n. (labeled as YPF1621) was published previously (Tashyreva et al. 2018a). BLAST query of the 16S rRNA gene sequence of the bacterial endosymbiont of *N. karyoxenos* revealed its α-proteobacterial origin with affiliation to Rickettsiales. We have therefore created a representative α-proteobacterial dataset with special focus on symbionts of protists and extended sampling of Rickettsiales, and aligned it using a local-pair algorithm as implemented in MAFFT 7 (Katoh and Standley 2013). Ambiguously aligned and hypervariable parts were then manually removed in Seaview 4 (Gouy et al. 2010). Edited alignment was subjected to maximum likelihood phylogenetic analysis under the Transversional model with equal base frequencies and six relaxed variable rates categories (TVMe + R6) in IQ-TREE 1.5 (Nguyen et al. 2015). This particular model was chosen as the best fitting according the Bayesian Information Criterion in model test implemented in IQ-TREE. Branching support was estimated from 1000 replicates using a thorough non-parametric bootstrap analysis in IQ-TREE. In addition, Bayesian posterior probabilities were inferred using the Phylobayes 4 (Lartillot and Philippe 2004) under empirical C20 mixture model with mutation rates defined

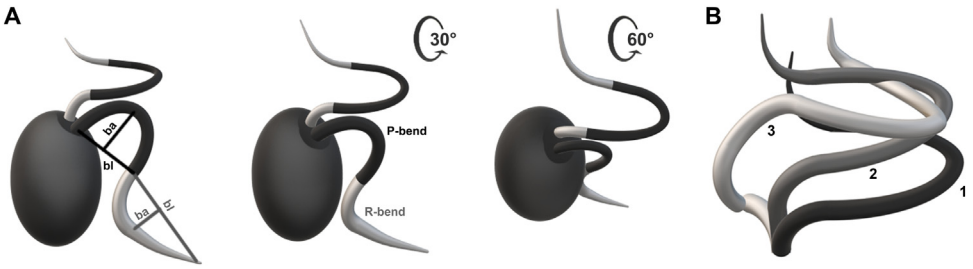

Figure 13. Diagram illustrating the flagellar bending pattern. (**A**) The measurements of bend amplitude (ba) and bend length (bl) are shown. The principal (P-bend) and the reverse (R-bend) bends are depicted in dark and light grey, correspondingly. (**B**) Drawing of dorsal flagellum displaying initiation of the bend and subsequent propagation in its own plane (successive positions from 1 to 3).

by GTR model. For this, two MCMC chains were run until they converged (i.e. maximum observed discrepancy between them was lower than 0.1 and effective number of model parameters reached at least 100). Probability of additional topologies of both hemistasiids as well as the bacterial symbiont of *N. karyoxenos* was tested using AU test in IQ-Tree with alternative branching force-constrained and analyzed also in IQ-Tree.

Light and fluorescence microscopy: A drop of cell suspension was placed between a glass slide and a coverslip and observed under the Olympus BX53 upright microscope equipped with differential interference contrast (DIC). Live cells were filmed with a DP72 digital camera at 1600 × 1200-pixel resolution using CellSens software v. 1.11 (Olympus). Video frames were processed using GIMP v. 2.8.14 and Irfan view v. 4.41. Image J v. 1.51 software was used for cell morphometry.

For fluorescence microscopy, pellets were fixed with 2% OsO_4 in seawater for 15 min, rinsed of the fixative and air-dried on glass slides. Adherent cells were permeabilized with 50, 80 and 100% ethanol and mounted in ProLong Gold antifade reagent (Life Technology) containing 4′,6-diamidino-2-phenylindole (DAPI). Slides were observed under the AxioPlan 2 fluorescence microscope (Carl Zeiss).

Electron microscopy: Cells were collected by centrifugation at 4,500 *g* for 20 min, either at the exponential phase of growth, or from cultures that were starved by incubation in artificial seawater alone for up to 15 days. For scanning electron microscopy (SEM), cell pellets were fixed with 1–2% OsO_4 in artificial seawater for 15 min at room temperature, washed 3 × 5 min in seawater diluted with distilled water (1:1) and adhered to a glass coverslip coated with 0.1% poly-*L*-lysine. Specimens were then dehydrated in an increasing gradient of acetone (30%–100%) for 15 min at each step, critical point dried using CO_2 and sprayed with gold in Sputter Coater Polaron chamber. Observations were performed using a JEOL 7401-F microscope at an accelerating voltage of 4 kV. For freeze-fracture electron microscopy, the samples were frozen in a high pressure freezer (Leica EMPACT 2) and transferred into a high vacuum preparation chamber (Gatan ALTO 2500). The frozen specimen was broken by a knife, and the exposed surface of the sample was preserved by sublimation at −98° C for 30 sec, then coated with a 3 nm layer of a platinum/palladium mixture at −135 °C. Images were obtained by Field Emission SEM JSM-7401F (JEOL) at an accelerating voltage of 1 kV. Transmission electron microscopy (TEM) samples were processed as described in Yurchenko et al. (2014). Micrographs were taken with an Olympus Mega View III camera using a JEOL 1010 TEM microscope operating at an accelerating voltage of 80 kV.

Cell motility: For observations, 30 μl of cell culture was transferred onto a microscope slide to make either an open drop or a thin film of between a slide and coverslip. Cell movements were recorded using a high-speed video camera i-SPEED TR (Olympus) with spatial resolution of 848 × 688 pixels and time resolution up to 1000 fps mounted on a BX50F microscope (Olympus) with either 40 × or 100 × positive phase-contrast objectives. All observations were made at 22 °C. A detailed analysis of the flagellar beating behavior and measurement of cell velocities was performed using the image analysis software Micro Image 4.0.1. (Olympus) as previously described in Prokopchuk et al. (2015). In brief, the bending patterns for one beat cycle were examined as shown on Figure 13. Flagellar beat frequency was calculated from the time interval between two successive wave initiations. Wave velocity was estimated from the change in distance between corresponding wave-crest points followed along the flagellum in successive images over time. Values of beating frequency and velocities are presented as averages, whereas bend amplitude and length are displayed as mean ± SD.

Acknowledgements

We thank Jan Votypka (Charles University, Prague) for help with the establishment of both cultures and Jiří Vaněček (Biology Centre) for assistance with freeze-fracture techniques. Support from the Czech Grant Agency 16-18699S, ERC CZ LL1601 and the ERD Funds, project OPVVV 16_019/0000759 to JL, the Czech Grant Agency 18-23787S to GP and AH, the Czech BioImaging grant (LM2015062) and ERDF (No. 16_013/0001775) to PM, and grant 17K19434 from the Japan Society for the Promotion of Science to AY is acknowledged. Work was partly undertaken in the Laboratory of Reproductive Physiology at the Research Institute of Fish Culture and Hydrobiology in Vodňany.

Appendix A. Supplementary Data

Supplementary data associated with this article can be found, in the online version, at https://doi.org/10.1016/j.protis.2019.04.001.

References

Adl SM, Bass D, Lane CE, Lukeš J, Schoch CL, Smirnov A, Agatha S, Berney C, Brown MW, Burki F, Cárdenas P, Čepička I, Chistyakova L, Del Campo J, Dunthorn M, Edvardsen B, Eglit Y, Guillou L, Hampl V, Heiss AA, Hoppenrath M, James TY, Karpov S, Kim E, Kolísko M, Kudryavtsev A, Lahr DJG, Lara E, Le Gall L, Lynn DH, Mann DG, Massana I Molera R, Mitchell EAD, Morrow C, Park JS, Pawlowski JW, Powell MJ, Richter DJ, Rueckert S, Shadwick L, Shimano S, Spiegel FW, Torruella I Cortes G, Youssef N, Zlatogursky V, Zhang Q (2019) Revision to the classification, nomenclature and diversity of eukaryotes. J Eukaryot Microbiol **66**:4–119

Al-Qassab S, Lee WJ, Murray S, Simpson AGB, Patterson DJ (2002) Flagellates from stromatolites and surrounding sediments in Shark Bay, Western Australia. Acta Protozool **41**:91–144

Bernard C, Simpson AGB, Patterson DJ (2000) Some free-living flagellates (Protista) from anoxic habitats. Ophelia **52**:113–142

Brugerolle G (1985) Des trichocystes chez les bodonids, un caractère phylogénétique supplémentaire entre Kinetoplastida et Euglenida. Protistologica **21**:339–348

Burger G, Valach M (2018) Perfection of eccentricity: mitochondrial genomes of diplonemids. IUBMB Life **70**:1197–1206

Cavalier-Smith T (2016) Higher classification and phylogeny of Euglenozoa. Europ J Protistol **56**:250–276

David V, Archibald JM (2016) Evolution: plumbing the depths of diplonemid diversity. Curr Biol **26**:R1290–R1292

de Vargas C, Audic S, Henry N, Decelle J, Mahé F, Logares R, Lara E, Berney C, Le Bescot N, Probert I, Carmichael M, Poulain J, Romac S, Colin S, Aury J-M, Bittner L, Chaffron S, Dunthorn M, Engelen S, Flegontova O, Guidi L, Horák A, Jaillon O, Lima-Mendez G, Lukeš J, Malviya S, Morard R, Mulot M, Scalco E, Siano R, Vincent F, Zingone A, Dimier C, Picheral M, Searson S, Kandels-Lewis S, Acinas SG, Bork P, Bowler C, Gorsky G, Grimsley N, Hingamp P, Iudicone D, Not F, Ogata H, Pesant S, Raes J, Sieracki ME, Speich S, Stemmann L, Sunagawa S, Weissenbach J, Wincker P, Karsenti E (2015) Eukaryotic plankton diversity in the sunlit ocean. Science **348**:1261605

Elbrächter M, Schnepf E (1998) Parasites of Harmful Algae. In Anderson DM, Cembella AD, Hallegraeff GM (eds) Physiological Ecology of Harmful Algal Blooms. Springer-Verlag, Berlin, pp 351–369

Elbrächter M, Schnepf E, Balzer I (1996) *Hemistasia phaeocysticola* (Scherffel) comb. nov., redescription of a free-living, marine, phagotrophic kinetoplastid flagellate. Arch Protistenkd **147**:125–136

Flegontov P, Gray MW, Burger G, Lukeš J (2011) Gene fragmentation: a key to mitochondrial genome evolution in Euglenozoa? Curr Genet **57**:225–232

Flegontova O, Flegontov P, Malviya S, Audic S, Wincker P, de Vargas C, Bowler C, Lukeš J, Horák A (2016) Extreme diversity of diplonemid eukaryotes in the ocean. Curr Biol **26**:3060–3065

Gawryluk RMR, Del Campo J, Okamoto N, Strassert JFH, Lukeš J, Richards TA, Worden AZ, Santoro AE, Keeling PJ (2016) Morphological identification and single cell genomics of marine diplonemids. Curr Biol **26**:3053–3059

Gouy M, Guindon S, Gascuel O (2010) SeaView Version 4: a multiplatform graphical user interface for sequence alignment and phylogenetic tree building. Mol Biol Evol **27**:221–224

Griessmann K (1913) Über marine Flagellaten. Arch Protistenkd **32**:1–78

Hausmann K (1978) Extrusive organelles in Protists. Int Rev Cytol **52**:197–276

Hughes LC, Ralston KS, Hill KL, Zhou ZH (2012) Three-dimensional structure of the trypanosome flagellum suggests that the paraflagellar rod functions as a biomechanical spring. PLoS ONE **7**:e25700

Katoh K, Standley DM (2013) MAFFT Multiple Sequence Alignment Software version 7: improvements in performance and usability. Mol Biol Evol **30**:772–780

Kiethega GN, Turcotte M, Burger G (2011) Evolutionarily conserved *cox1* trans-splicing without cis-motifs. Mol Biol Evol **28**:2425–2428

Kivic PA, Walne PL (1984) An evaluation of a possible phylogenetic relationship between the Euglenophyta and Kinetoplastida. Orig Life Evol Biosph **13**:269–288

Lara E, Moreira D, Vereshchaka A, López-García P (2009) Pan-oceanic distribution of new highly diverse clades of deep-sea diplonemids. Environ Microbiol **11**:47–55

Larsen J, Patterson DJ (1990) Some flagellates (Protista) from tropical marine sediments. J Nat Hist **24**:801–937

Lartillot N, Philippe H (2004) A Bayesian mixture model for across-site heterogeneities in the amino-acid replacement process. Mol Biol Evol **21**:1095–1109

Leander BS (2004) Did trypanosomatid parasites have photosynthetic ancestors? Trends Microbiol **12**:251–258

Leander BS, Esson HJ, Breglia SA (2007) Macroevolution of complex cytoskeletal systems in euglenids. Bioessays **29**:987–1000

Lee WJ (2002) Redescription of the rare heterotrophic flagellate (Protista) – *Phyllomitus undulans* Stein 1878, and erection of a new genus – *Pseudophyllomitus* gen. n. Acta Protozool **41**:375–382

Lee WJ (2015) Small free-living heterotrophic flagellates from marine sediments of Gippsland Basin, South-Eastern Australia. Acta Protozool **54**:53–76

Lukeš J, Flegontova O, Horák A (2015) Diplonemids. Curr Biol **25**:R702–R704

Lukeš J, Wheeler R, Jirsová D, David V, Archibald JM (2018) Massive mitochondrial DNA content in diplonemid and kinetoplast protists. IUBMB Life **70**:1267–1274

Marande W, Burger G (2007) Mitochondrial DNA as a genomic jigsaw puzzle. Science **318**:415

Mignot JP (1966) Structure et ultrastructure de quelques euglénomonadines. Protistologica **2**:51–117

Mignot J-P, Hovasse R (1973) Nouvelle contribution a la connaissance des trichocystes:les organites grilladés d'*Entosiphon sulcatum* (Flagellata, Euglenida). Protistologica **9**:373–391

Montegut-Felkner AE, Triemer RE (1994) Phylogeny of *Diplonema ambulator* (Larsen and Patterson): 1. Homologies of the flagellar apparatus. Europ J Protistol **30**:227–237

Montegut-Felkner AE, Triemer RE (1996) Phylogeny of *Diplonema ambulator* (Larsen and Patterson). 2. Homologies of the feeding apparatus. Europ J Protistol **32**:64–76

Mylnikov AP, Mylnikova ZM, Tsvetkov AH, Elizarova VA (1998) Fine structure of the predatory flagellate *Phyllomitus amylophagus* (in Russian). Biol Vnutr Vod **2**:21–27

Nguyen L-T, Schmidt HA, von Haeseler A, Minh BQ (2015) IQ-TREE: a fast and effective stochastic algorithm for estimating maximum-likelihood phylogenies. Mol Biol Evol **32**:268–274

Okamoto N, Gawryluk RMR, del Campo J, Strassert JFH, Lukeš J, Richards TA, Worden AZ, Santoro AE, Keeling PJ (2019) A revised taxonomy of diplonemids including the Eupelagonemidae n. fam. and a type species, *Eupelagonema oceanica* n. gen. & sp. J Eukaryot Microbiol **66**:519–524

Pavillard J (1922) *Pronoctiluca et Noctiluca*. Bull Soc Bot France **69**:365–370

Porter D (1973) *Isonema papillatum* sp. n., a new colorless marine flagellate: a light- and electronmicroscopic study. J Protozool **20**:351–356

Prokopchuk G, Dzyuba B, Bondarenko O, Rodina M, Cosson J (2015) Motility initiation of sterlet sturgeon (*Acipenser ruthenus*) spermatozoa: describing the propagation of the first flagellar waves. Theriogenology **84**:51–61

Roy J, Faktorová D, Benada O, Lukeš J, Burger G (2007) Description of *Rhynchopus euleeides* n. sp. (Diplonemea), a free-living marine euglenozoan. J Eukaryot Microbiol **54**:137–145

Scherffel A (1900) *Phaeocystis globosa* nov. spec. nebst einigen Betrachtungen über die Phylogenie niederer, insbesondere brauner Organismen. Wiss Meeresunters Abt Helgoland **4**:1–29

Schiller J (1925) Über die Besiedlung europäischer Meere mit Cryptomonaden und über einen Flagellaten peridineenähnlicher Organisation (*Entomosigma peridinioides*). Österr Bot Ztschr **74**:194–198

Schnepf E (1994) Light and electron microscopical observations in *Rhynchopus coscinodiscivorus* spec. nov., a colorless, phagotrophic Euglenozoon with concealed flagella. Arch Protistenknd **144**:63–74

Schulz F, Horn M (2015) Intranuclear bacteria: Inside the cellular control center of eukaryotes. Trends Cell Biol **25**:339–346

Schuster FL, Goldstein S, Hershenov B (1968) Ultrastructure of a flagellate *Isonema nigricans* nov. gen. nov. sp., from a polluted marine habitat. Protistologica **4**:141–149

Senn G (1911) *Oxyrrhis*, *Nephroselmis* und einige Euflagellaten, nebst Bemerkungen über deren System. Zschr wiss Zool **97**:605–672

Simpson AGB (1997) The identity and composition of the Euglenozoa. Arch Protistenkd **148**:318–328

Simpson AGB, Roger AJ (2004) Protein phylogenies robustly resolve the deep-level relationships within Euglenozoa. Mol Phylogenet Evol **30**:201–212

Simpson AGB, van den Hoff J, Bernard C, Burton HR, Patterson DJ (1997) The ultrastructure and systematic position of the euglenozoon Postgaardi mariagerensis, Fenchel et al. Arch Protistenkd **147**:213–225

Szokoli F, Sabaneyeva E, Castelli M, Krenek S, Schrallhammer M, Soares CAG, Da Silva-Neto ID, Berendonk TU, Petroni G (2016) "*Candidatus* Fokinia solitaria", a novel "stand-alone" symbiotic lineage of Midichloriaceae (Rickettsiales). PLoS ONE **11(1)**:e0145743

Tashyreva D, Prokopchuk G, Yabuki A, Kaur B, Faktorová D, Votýpka J, Kusaka C, Fujikura K, Shiratori T, Ishida KI, Horák A, Lukeš J (2018a) Phylogeny and morphology of new diplonemids from Japan. Protist **169**:158–179

Tashyreva D, Prokopchuk G, Votýpka J, Yabuki A, Horák A, Lukeš J (2018b) Life cycle, ultrastructure, and phylogeny of new diplonemids and their endosymbiotic bacteria. mBio **9(2)**:e02447-17

Throndsen J (1969) Flagellates of Norwegian coastal waters. Nytt Mag Bot **16**:161–216

Triemer RE (1992) Ultrastructure of mitosis in Diplonema ambulator Larsen & Patterson (Euglenozoa). Europ J Protistol **28**:398–404

Triemer RE, Farmer MA (1991) An ultrastructural comparison of the mitotic apparatus, feeding apparatus, flagellar apparatus and cytoskeleton in euglenoids and kinetoplastids. Protoplasma **28**:398–404

Triemer RE, Ott DW (1990) Ultrastructure of Diplonema ambulator Larsen & Patterson (Euglenozoa) and its relationship to Isonema. Europ J Protistol **25**:316–320

Valach M, Moreira S, Faktorova D, Lukeš J, Burger G (2016) Post-transcriptional mending of gene sequences: looking under the hood of mitochondrial gene expression in diplonemids. RNA Biol **13**:1204–1211

Vickerman K (2000) Diplonemids (Class: Diplonemea Cavalier Smith, 1993). In Lee JJ, Leedale GF, Bradbury P (eds) An Illustrated Guide to the Protozoa **Vol. 2**, 2nd edn Society of Protozoologists, Lawrence, Kansas, USA, pp 1157–1159

von der Heyden S, Chao EE, Vickerman K, Cavalier-Smith T (2004) Ribosomal RNA phylogeny of bodonid and diplonemid flagellates and the evolution of Euglenozoa. J Eukaryot Microbiol **51**:402–416

Vørs N (1992) Heterotrophic amoebae, flagellates and heliozoa from the Tvärminne area, Gulf of Finland, in 1988–1990. Ophelia **36**:1–109

Yabuki A, Tame A (2015) Phylogeny and reclassification of *Hemistasia phaeocysticola* (Scherffel) Elbrächter & Schnepf, 1996. J Eukaryot Microbiol **62**:426–429

Yabuki A, Tanifuji G, Kusaka C, Takishita K, Fujikura K (2016) Hyper-eccentric structural genes in the mitochondrial genome of the algal parasite *Hemistasia phaeocysticola*. Genome Biol Evol **8**:2870–2878

Yubuki N, Edgcomb VP, Bernhard JM, Leander BS (2009) Ultrastructure and molecular phylogeny of *Calkinsia aureus*: cellular identity of a novel clade of deep-sea euglenozoans with epibiotic bacteria. BMC Microbiol **9**:16

Yurchenko V, Votýpka J, Tesařová M, Klepetková H, Kraeva N, Jirků M, Lukeš J (2014) Ultrastructure and molecular phylogeny of four new species of monoxenous trypanosomatids from flies (Diptera: Brachycera) with redefinition of the genus *Wallaceina*. Folia Parasitol **61**:97–112